MULTISCALE MODEL. SIMUL.
Vol. 10, No. 3, pp. 874–905

SINGLE AND TWO-SCALE SHARP-INTERFACE MODELS FOR CONCRETE CARBONATION—ASYMPTOTICS AND NUMERICAL APPROXIMATION*

JONATHAN D. EVANS†, ANDREA FERNÁNDEZ†, AND ADRIAN MUNTEAN‡

Abstract. We investigate the fast-reaction asymptotics for a one-dimensional reaction-diffusion system describing the penetration of the carbonation reaction in concrete. The technique of matched-asymptotics is used to show that the reaction-diffusion system leads to two distinct classes of sharp-interface models. These correspond to different scalings of a small parameter ϵ representing the fast-reaction and defined here as the ratio between the characteristic scale of diffusion for the fastest species and the characteristic scale of the carbonation reaction. We explore three conceptually different diffusion regimes in terms of the behavior of the effective diffusivities for the driving chemical species. The limiting models include one-phase and two-phase generalized Stefan moving-boundary problems as well as a nonstandard two-scale (micro-macro) moving-boundary problem—the main result of the paper. Numerical results, supporting the asymptotics, illustrate the behavior of the concentration profiles for relevant parameter regimes.

Key words. concrete carbonation, reaction layer analysis, matched asymptotics, fast-reaction asymptotics, two-scale sharp-interface models, numerical approximation of reaction fronts

AMS subject classifications. 35K57, 41A60, 92E20, 80A30, 65M60

DOI. 10.1137/110859701

1. Introduction.

Carbonation reactions alter the concrete's pore geometry in a difficult-to-control fashion. A good theoretical multiscale understanding of the evolution of carbonation reactions in such a complex multiphase material is vital towards obtaining accurate predictions of the durability of large concrete structures (see, for example, [17, 4]). Having a good estimate of the life service of motorways, bridges, sewage pipe systems (etc.) can save significant amounts of money and energy yearly—hence the growing multidisciplinary research interest in this topic.

1.1. Background.

From the point of view of the involved geochemistry, the process of concrete carbonation mainly involves the reaction of atmospheric carbon dioxide with calcium hydroxide found in the pore solution to form water and calcium carbonate. The pore solution is highly alkaline (pH$\sim$14), and as soon as the pH level decreases, the microscopic oxide layer at the steel reinforcements disappears and the steel can corrode. This corrosion causes the durability of the structure to reduce dramatically. Figure 1 shows how the pH levels of the concrete block drop dramatically. For more details on concrete carbonation and its relevance with respect to corrosion and durability issues, we refer the reader to [29, 17, 6] as well as to the references cited therein.

*Received by the editors December 20, 2011; accepted for publication (in revised form) April 30, 2012; published electronically August 8, 2012.
http://www.siam.org/journals/mms/10-3/85970.html
†Department of Mathematical Sciences, University of Bath, Bath, BA2 7AY, UK (masjde@maths.bath.ac.uk, af243@bath.ac.uk).
‡Center for Analysis, Scientific Computing and Applications (CASA), Department of Mathematics and Computer Science, Institute for Complex Molecular Systems (ICMS), Eindhoven University of Technology, PO Box 513, 5600 MB Eindhoven, The Netherlands (a.muntean@tue.nl). This author's work was partially supported by DFG SPP1122.

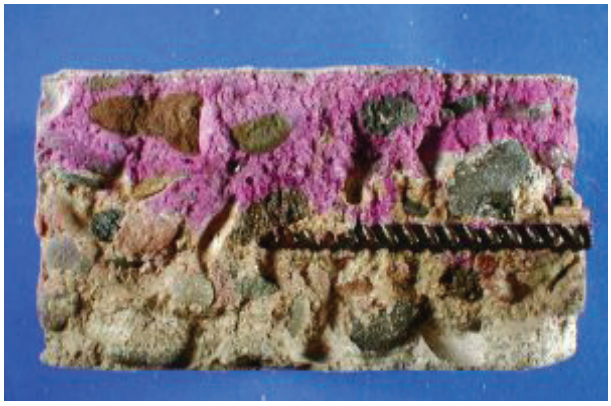

FIG. 1. *Cross section of a reinforced concrete block. Pink indicates low pH, while colorless indicates a high one.*

Here, we focus on the dominant carbonation reaction mechanism, namely

$$\mathrm{CO_2}(g \to aq) + \mathrm{Ca(OH)_2}(s \to aq) \to \mathrm{CaCO_3}(aq \to s) + \mathrm{H_2O}. \tag{1}$$

In other words, atmospheric carbon dioxide diffuses through the unsaturated concrete matrix and dissolves into the pore water, while the calcium hydroxide is available in the pore solution by dissolution from the solid matrix. Free water and calcium carbonate are the main reaction products in (1). $CaCO_3$ quickly precipitates into the solid matrix, while the water diffuses through the material very much influenced by eventual wetting and deleting cycles. As a consequence of so many reaction and transport mechanisms, the available macroscopic models capturing carbonation in concrete are complex and involve a large number of parameters. For this reason, although the mechanisms are rather well understood, the predictive power of such models is questionable. The challenge is to find minimal models that can accurately predict CO_2 penetration depths in concrete.

Our objective is to understand how fast the reaction (1) moves into the material, driven by CO_2 diffusion. In other words, we want to use a detailed reaction layer analysis to determine the speed of growth of the macroscopic carbonated phase (the pink region in Figure 1). The output of our approach/models consists of carbonation penetration depths and profiles of active concentrations.

In this context, the open question is:

(Q) *Which boundary conditions need to be imposed at the reaction interface to describe its correct motion?*

(Q) has been recently addressed, for instance, in [21, 25, 2, 24, 23, 3, 22] and [26], where the authors indicate that the answer seems to be rather well understood in one space dimension. However, the two- and three-dimensional cases are comparatively untouched. The reason for this is simple: For the moment, one does not know how the reaction front (hosting (1)) feels the presence of corners or more complex geometrical shapes. Furthermore, the mathematical theory of free boundary problems (FBPs) in more space dimensions (and posed in heterogeneous media) is less understood. Rigorous results are mostly available for standard FBPs, relying heavily on a priori prescribed regularity for the moving boundary (sharp interface). For practical purposes, we require robust models (ϵ-approximations of sharp-interface models for carbonation) that are appropriate in any space dimension. Such models should

not require any special regularity requirements on the sharp interface and should be able to capture as $\epsilon \to 0$ the correct moving interface conditions. This is the place in which our paper contributes. The research reported here is preliminary, with our main asymptotic results emphasizing a new, nonstandard, two-scale sharp-interface model. Many associated fundamental and practical issues are currently open (see section 8) and deserve further study.

1.2. Approach. We introduce a basic macroscopic reaction-diffusion model to describe the aqueous chemistry and transport involved in (1). To be more precise, we consider only the concentration of the reactants $CO_2(aq)$ and $Ca(OH)_2(aq)$, both of which we allow to diffuse. Furthermore, we assume that the diffusion coefficients can be concentration dependent and also may vary with the reaction rate. We then use the technique of matched-asymptotics [5] to perform a detailed analysis of the reaction layer for various physically relevant scaling regimes. Additionally, we use COMSOL multiphysics to produce numerical results of the original system that corroborate the asymptotic results obtained for the various scaling cases.

Since we look to carbonation in high Thiele moduli regimes, the rate at which the concentrations diffuse is much slower than that of the reaction. Thus we focus on the *fast reaction limit* $\epsilon \to 0$, where $\epsilon > 0$ is a scale parameter that will be explained in the next section. Assuming strong separation of time scales, the reaction is expected to be in equilibrium except for an interior narrow layer[1] where virtually all the reaction takes place. The structure of this localized reaction zone is sensitive to the behavior of the diffusion coefficients. For this reason, we investigate three different possible situations in regard to the diffusivities. These lead to the derivation of conceptually different sharp-interface models. We see three main types: namely, one- and two-phase Stefan-like problems with zero latent heat, and two-scale micro-macro FBPs. The latter is a completely new type of model in which the speed of the reaction interface is updated from a smaller length scale.

The broad spectrum of different models shown here not only depicts the behavior of the concentrations for many possible scenarios of carbonation, but can also be related to other types of aggressive reactions like redox scenarios [15], silicon-oxidation [10], sulfate attack [1, 13, 27], and combustion [14]. The techniques used here are therefore applicable to a larger set of reaction-diffusion problems.

1.3. Organization of the paper. The macroscopic reaction-diffusion system modeling carbonation is introduced in section 2. Performing our fast-reaction asymptotics, a first sharp-interface model is derived in section 3. The bulk of the paper (sections 4, 5, and 6) is devoted to the reaction layer analysis for three different diffusion coefficient regimes. The first regime (section 4) is that in which the diffusion coefficients remain order 1, which we refer to as slowly varying. This is the usual case which has received attention in the literature. The other regimes allow the diffusion coefficients to change their orders of magnitude in terms of the parameter ϵ, the diffusion coefficients then being termed rapidly varying. Thus, as a second regime (section 5) we consider only a rapidly varying CO_2 diffusivity, with the hydroxide diffusivity slowly varying. Finally, as a third regime (section 6), we consider the effects of rapidly varying CO_2 and hydroxide diffusivities simultaneously. The main results of the paper are the two-scale sharp-interface models, which are summarized

[1] Interestingly, the strong separation of the characteristic time scales of diffusion and reaction leads to the presence of two distinct (macroscopic) characteristic space scales that relate to the typical sizes of the layers hosting diffusion and reaction.

in section 7. The specific generalized Stefan and kinetic conditions on the moving boundary are summarized for the single and two rapidly varying cases in sections 5.3 and 6.3, and should be compared to the conditions in the slowly varying case in section 4.3. Each regime subdivides according to the size of a relative transport parameter, which measures the characteristic ratio of diffusivities and concentrations for CO_2 and hydroxide.

We close the paper with a discussion section around possible connections between the nonstandard two-scale models derived in this paper and the two-scale models obtained previously in the homogenization literature [16].

2. The model equations. We consider the concrete occupying a one-dimensional slab geometry $\Omega :=]0, L[$. The x-axis is directed into the concrete, with the surface $x = 0$ being exposed to an external source of CO_2, while the surface $x = L$ is assumed impervious to all reaction species. We let $c = c(x,t)$ and $h = h(x,t)$ denote the concentrations of CO_2(aq) and $Ca(OH)_2$(aq), respectively, expressed as moles per unit volume (i.e., the intrinsic concentrations). We adopt the following set of reaction-diffusion equations:

$$\text{in } 0 < x < L,\ t > 0, \qquad \frac{\partial c}{\partial t} = \frac{\partial}{\partial x}\left(D_c \frac{\partial c}{\partial x}\right) - R(c,h), \tag{2}$$

$$\frac{\partial h}{\partial t} = \frac{\partial}{\partial x}\left(D_h \frac{\partial h}{\partial x}\right) - R(c,h), \tag{3}$$

with boundary conditions

$$\text{on } x = 0, \qquad -D_c \frac{\partial c}{\partial x} = H^*(c^* - c), \quad \frac{\partial h}{\partial x} = 0, \tag{4}$$

$$\text{on } x = L, \qquad \frac{\partial c}{\partial x} = 0, \quad \frac{\partial h}{\partial x} = 0, \tag{5}$$

and initial conditions

$$\text{at } t = 0, \qquad c = c^* c_i(x), \quad h = h^0 h_i(x). \tag{6}$$

The initial hydroxide concentration has a representative value (taken as maximum) denoted by the constant h^0, the most common situation being $h_i(x) = 1$, $c_i(x) = 0$ for $0 \le x \le L$. Here the concrete substrate has length L; R is the carbonation rate with reaction rate coefficient k; and D_c and D_h are the diffusion coefficients of CO_2 and $Ca(OH)_2$, respectively, which are not necessarily constant. Not only can the diffusion coefficients be concentration dependent[2] but also we allow them to vary with the reaction rate. Motivation for this comes from the significant change that takes place in the concrete matrix during carbonation. The main modeling assumption is thus to consider their dependence linked to $R(c,h)$, which for specificity may be taken in Arrhenius forms,

$$D_i = D_i^0 \left(1 - \exp\left(-\frac{\nu_i}{R_i}\right)\right), \qquad i = c, h, \tag{7}$$

[2]Consider the diffusion coefficient of CO_2; this may be expressed as $D_c = \hat{D}_c w \Phi(h)$, where w is a tortuosity factor and $\Phi(h)$ is the porosity, which depends on the concentration of $Ca(OH)_2$. This gives a justification for the $Ca(OH)_2$ dependence of the diffusivity. We refer the reader to [21] for more remarks in this direction.

ν_c, ν_h suitable constants, and R_c, R_h based on partial reaction rates. We note that neither the effective diffusivities nor the reaction rate coefficient depend on humidity. Also the transfer of CO_2 from the air to water phase (and vice versa) and the dissolution of $Ca(OH)_2$ from the solid matrix to water phase (and vice versa) are in local equilibrium; i.e., all production terms by Henry's law vanish; see [7] for more details on molecular transfer across water-air interfaces and on Henry's law. As such, from a modeling perspective, we may justify the Robin boundary condition for the aqueous carbon dioxide in (4) as follows. Denoting the concentration of gaseous carbon dioxide CO_2(g) in the concrete by c_g with diffusion coefficient D_{c_g}, its exchange with the external atmospheric concentration c_g^* at the exposed concrete surface is given by

$$\text{at } x = 0, \qquad -D_{c_g}\frac{\partial c_g}{\partial x} = H_g^*(c_g^* - c_g),$$

where H_g^* is the mass transfer constant. Assuming an equilibrium balance $c = C^H c_g$ for the local exchange of gaseous and aqueous carbon dioxide, we may combine these expressions to give (4), where

$$H^* = \frac{H_g^* D_c}{D_{c_g}}, \qquad c^* = C^H c_g^*.$$

The dimensionless Henry constant C^H is temperature dependent, a typical value being 0.82 at 20°C. We remark that the assumption of equilibrium balance between gaseous and aqueous carbon dioxide means that D_c should be taken as D_{c_g}, the governing equation (2) then being consistent with the models of [29, 30] when written in terms of c_g. More sophisticated models may relax this equilibrium assumption, allowing CO_2 in the gas and aqueous phases to be considered separately.

The formation of calcium carbonate (concentration $z(x,t)$) can be modeled using the rate equation

$$\frac{\partial z}{\partial t} = R(c,h), \tag{8}$$

where its diffusivity is taken as being negligible. As such, the amount of carbonate can be determined once (2)–(6) is solved together with specifying a suitable initial condition, e.g., $z = 0$ at $t = 0$.

We nondimensionalize as follows:

$$x = L\bar{x}, \quad t = \frac{L^2 h^0}{D_c^0 c^*}\bar{t}, \quad c = c^*\bar{c}, \quad h = h^0\bar{h},$$
$$D_c = D_c^0\bar{D}_c, \quad D_h = D_h^0\bar{D}_h, \quad R(c,h) = \theta r(\bar{c},\bar{h}),$$

using L as the characteristic length scale and θ as a representative reaction rate scaling. We have taken D_c^0 and D_h^0 as the maximum values of the diffusion coefficients. Dropping $^-$'s, we obtain

$$\text{in } 0 < x < 1,\ t > 0, \qquad \epsilon^2\left(\mu\frac{\partial c}{\partial t} - \frac{\partial}{\partial x}\left(D_c\frac{\partial c}{\partial x}\right)\right) = -r(c,h), \tag{9}$$

$$\epsilon^2\left(\frac{\partial h}{\partial t} - \frac{\delta^2}{\epsilon^2}\frac{\partial}{\partial x}\left(D_h\frac{\partial h}{\partial x}\right)\right) = -r(c,h), \tag{10}$$

TABLE 1

Typical parameter values for natural and accelerated[3] *carbonation obtained from* [20, 31, 29, 30]. *Concentrations are expressed in units of mol* m^{-3} *for consistency with the reaction rate (partial orders of the reaction being* $p = q = 1$*); the molar masses of* $44.01g$ *for* CO_2 *and* $74g$ *for* $Ca(OH)_2$ *may be used to convert to units of* $g\ m^{-3}$.

Parameter (units)	Value (accelerated)	Value (natural)
$D_c^0 = D_{c_g}^0$ $(\mathrm{m^2 s^{-1}})$	$(0.5-5)\times 10^{-8}$	$(0.5-5)\times 10^{-8}$
D_h^0 $(\mathrm{m^2 s^{-1}})$	10^{-13}	10^{-13}
H_g^* $(\mathrm{m\ s^{-1}})$	1.16×10^{-2}	1.16×10^{-2}
c^* $(\mathrm{mol\ m^{-3}})$	4.38	2.71×10^{-3}
h^0 $(\mathrm{mol\ m^{-3}})$	1.04×10^{3}	1.04×10^{3}
k $(\mathrm{m^3 mol^{-1} s^{-1}})$	1.74×10^{-5}	4.6×10^{-5}

with boundary conditions

$$\text{on } x=0, \qquad -D_c\frac{\partial c}{\partial x} = H(1-c), \quad \frac{\partial h}{\partial x} = 0, \tag{11}$$

$$\text{on } x=1, \qquad \frac{\partial c}{\partial x} = 0, \quad \frac{\partial h}{\partial x} = 0, \tag{12}$$

and initial conditions

$$\text{at } t=0, \qquad c = c_i(x), \quad h = h_i(x), \tag{13}$$

where

$$\epsilon^2 = \frac{D_c^0 c^*}{L^2\theta}, \qquad \delta^2 = \frac{D_h^0 h^0}{L^2\theta}, \qquad \mu = \frac{c^*}{h^0}, \qquad H = \frac{LH^*}{D_c^0}. \tag{14}$$

In the semi-infinite concrete case, L is at our disposal and can be taken to be D_c^0/H^* so that $H = 1$ (when H^* is finite).

The scaling θ is chosen so that $r(c,h) \le 1$ for $0 \le c \le 1$, $0 \le h \le 1$. To be more precise, for reaction terms of the form

$$R(c,h) = kc^p h^q,$$

where k is a constant reaction coefficient and p and q are positive constants, we have

$$r(c,h) = c^p h^q \tag{15}$$

by choosing $\theta = k(c^*)^p (h^0)^q$. Referring to [32] and [20], typical values of the dimensional parameters are given in Table 1. A representative length L can be of the order of cm up to several meters, i.e., $L = 0.1$–10m, depending upon the situation and geometry considered. The quoted reaction rate corresponds to the common partial reaction orders $p = q = 1$, although we mention that other values $0.9 \le p, q \le 1.5$ also seem appropriate. These give the estimates shown in Table 2 for the dimensionless parameters. The parameter range of relevance is thus

$$\epsilon \ll 1, \qquad \delta \le O(\epsilon), \qquad \mu \ll 1, \qquad H = O(1), \tag{16}$$

[3]Natural environments normally contain 0.03–0.05% CO_2, with the evolution of the carbonation depth being slow and taking many years (typically 5–10 years). An accelerated carbonation chamber exposes concrete to 50% CO_2, which dramatically reduces the time needed to perform experiments from years to a matter of days (typically up to 20 days).

TABLE 2
Estimated nondimensional parameters using values in Table 1.

Nondimensional parameter	Value (accelerated)	Value (natural)
ϵ^2	10^{-9}–10^{-4}	10^{-9}–10^{-4}
δ^2	10^{-11}–10^{-7}	10^{-10}–10^{-5}
μ	10^{-3}	10^{-6}
H	10^{4}–10^{7}	10^{4}–10^{7}

where we note that the "relative transport parameter,"

$$\frac{\delta^2}{\epsilon^2} = \frac{D_h^0 h^0}{D_c^0 c^*}, \tag{17}$$

is typically small or at most order 1 [29]. The CO_2 interfacial exchange parameter H is estimated using the maximum values of the CO_2 diffusivities, which are expected to occur at the surface and which for gas are denoted by $D_{c_g}^0$. Since $D_c^0 = D_{c_g}^0$ we have that $H = LH_g^*/D_{c_g}^0$, the larger values of this parameter suggesting that the interfacial exchanges are close to equilibrium. The diffusion coefficients now have dependencies on the parameters ϵ and δ, i.e., $D_c = D_c(c, h; \epsilon)$, $D_h = D_h(c, h; \delta)$ being the general form. As far as this paper is concerned, we focus on the simpler dependency cases $D_c(h; \epsilon), D_h(c; \epsilon)$ with extensions being straightforward. For instance, the functional forms (7) become

$$D_c = 1 - \exp\left(-\frac{\nu_1 \epsilon^2}{h^q}\right), \qquad D_h = 1 - \exp\left(-\frac{\nu_2 \delta^2}{c^p}\right), \tag{18}$$

where $\nu_1 \epsilon^2 = \nu_c / h_0^q$, $\nu_2 \delta^2 = \nu_h / c^{*p}$ on taking $R_c = h^q$, $R_h = c^p$.

3. The sharp-interface model derivation. The limit $\epsilon \to 0$ will be considered; Ortoleva et al. [28] (cf. section E, p. 1001) refer to this as the fast-aqueous-reaction asymptotics. This corresponds to the bulk reaction being very rapid, with the reaction essentially in equilibrium ($c = 0$ or $h = 0$ at leading order in ϵ) except in a thin boundary layer, the reaction zone, where virtually all the carbonation occurs. In other words, almost all the reaction is confined to a very narrow layer, the structure of which will be sensitive to the behavior of the diffusion coefficients. The location of the reaction zone will be denoted by $x = s(t; \epsilon)$, which here is taken as a suitable point within its center. Its specification is not unique. Since our reaction species have monotonic concentration profiles, for definiteness we take $s(t; \epsilon)$ as the position where the concentrations of CO_2 and $Ca(OH)_2$ cross, i.e.,

$$s(t; \epsilon) = \{x \in [0, L] \mid c(x, t) = h(x, t)\}.$$

As the reaction zone is very thin, $s(t; \epsilon)$ may be used to represent the position of the carbonation reaction front. In the literature there are alternative ways of defining such a front (see the discussion in [20]), a common one using the degree of local carbonation as represented through a suitable high concentration isoline of the reaction product $CaCO_3$. These alternative definitions should be equivalent to within the thickness of the reaction zone. We denote the regions in which the reaction is in equilibrium as the outer regions, where outer 1 has $h = o(1)$ and outer 2 has $c = o(1)$. The details of the reaction zone depend crucially on the behavior of the diffusion coefficients, which

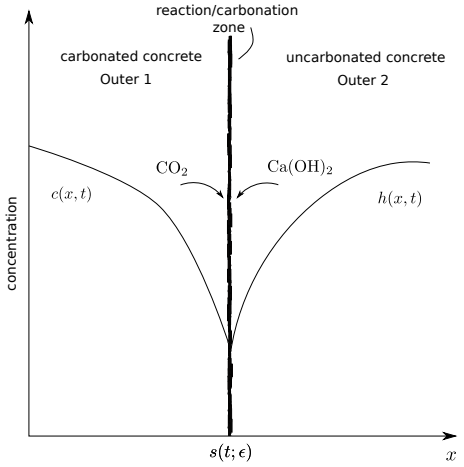

FIG. 2. *A schematic illustration of the carbonation process in concrete. CO_2 enters the concrete and diffuses to the reaction (or carbonation) zone, where it rapidly reacts with $Ca(OH)_2$. Shown qualitatively are the concentration profiles $c(x,t)$, $h(x,t)$ and the reaction zone position $s(t;\epsilon)$ at a fixed time t. The asymptotic structure of the reaction zone depends upon the properties of the diffusivities. It can be just a single region (as for the slowly varying diffusivities in section 4) or have more than one region (as described in sections 5 and 6 for rapidly varying diffusivities).*

we investigate in subsequent sections. Figure 2 illustrates schematically the situation. For generality of derivation, we keep $\mu = O(1)$ and consider its vanishing limit later when seeking to solve the resulting sharp-interface Stefan problems.

3.1. Outer solutions. Taking the limit $\epsilon \to 0$ and posing regular expansions

$$c = c_0 + O(\epsilon^2), \qquad h = h_0 + O(\epsilon^2),$$

we obtain two outer regions as below. The location of the reaction zone also requires expansion; the leading order term we denote by $s(t)$, the higher order terms not impacting in the analysis to the orders of the calculations considered.

Outer 1. $0 < x < s(t)$ (carbon dioxide region). Here we have $h_0 = 0$ (with, in fact, $h = 0$ to all algebraic orders of ϵ) and

$$\mu \frac{\partial c_0}{\partial t} - \frac{\partial}{\partial x}\left(D_{c_0} \frac{\partial c_0}{\partial x} \right) = 0, \tag{19}$$

where $D_{c_0} = D_c(c_0, 0; 0)$. This region is essentially calcium hydroxide-free, it having been used up in the reaction to form calcium carbonate.

Outer 2. $s(t) < x < 1$ (calcium hydroxide region). In this region we have $c_0 = 0$ (and, in fact, $c = 0$ to all algebraic orders in ϵ) with

$$\frac{\partial h_0}{\partial t} - \frac{\delta^2}{\epsilon^2} \frac{\partial}{\partial x}\left(D_{h_0} \frac{\partial h_0}{\partial x} \right) = 0, \tag{20}$$

with $D_{h_0} = D_h(0, h_0; 0)$. This equation may simplify further, depending upon the relative sizes of δ and ϵ. This region is almost pure calcium hydroxide, the presence of carbon dioxide being negligible.

3.2. Interface conditions. In practical terms it is the outer regions that are the ones of most significance; however, the interior layer must be analyzed to obtain the continuity conditions linking both outers. Without appealing to such an inner analysis, however, we can use (9) and (10) to obtain the statement

$$\frac{\partial}{\partial t}(\mu c - h) = \frac{\partial}{\partial x}\left(D_c \frac{\partial c}{\partial x} - \frac{\delta^2}{\epsilon^2} D_h \frac{\partial h}{\partial x}\right). \tag{21}$$

This may now be used to obtain the jump condition at $x = s(t)$,

$$\left[D_c \frac{\partial c}{\partial x} - \frac{\delta^2}{\epsilon^2} D_h \frac{\partial h}{\partial x} + \dot{s}(\mu c - h)\right]_{s_-}^{s_+} = 0, \tag{22}$$

representing conservation of mass. Using the outer solutions, this yields

$$\text{at } x = s(t), \quad -D_{c_0} \frac{\partial c_0(s^-, t)}{\partial x} - \frac{\delta^2}{\epsilon^2} D_{h_0} \frac{\partial h_0(s^+, t)}{\partial x} = \dot{s}(\mu c_0(s^-, t) + h_0(s^+, t)). \tag{23}$$

This represents the Stefan-type moving-boundary condition for (19) and (20). However, we still remain two conditions short in terms of specifying the moving-boundary problem. These final conditions can be found only by undertaking an interior layer analysis of the reaction zone. They correspond to kinetic conditions and will take the general form

$$c_0(s^-, t) = \Phi_1(\dot{s}), \qquad h_0(s^+, t) = \Phi_2(\dot{s}), \tag{24}$$

where the functions Φ_1 and Φ_2 are to be determined. To complete the sharp-interface statement we require suitable initial conditions. These are parameter-sensitive, the most usual situation being

$$\begin{aligned} \text{at } t = 0, \qquad & c_0 = c_i(x) \quad \text{for } 0 < x < s(0), \\ & h_0 = h_i(x) \quad \text{for } s(0) < x < 1 \text{ and } s(0) = s_0, \end{aligned} \tag{25}$$

with, more often than not, the initial position of the reaction zone being taken at the concrete surface $s_0 = 0$. In certain parameter regimes, there is an initial carbonation stage in which the reaction zone remains in its initial location for a finite time t_0. In the this case we modify (25) to

$$\begin{aligned} \text{at } t = t_0, \qquad & c_0 = C_i(x) \quad \text{for } 0 < x < s(0), \\ & h_0 = H_i(x) \quad \text{for } s(0) < x < 1 \text{ and } s(0) = s_0, \end{aligned} \tag{26}$$

where C_i and H_i are the resulting concentration profiles at the end of this initial carbonation stage.

The moving-boundary problem (19)–(20), (23)–(24), with (25) or (26) is a two-phase problem in the regime $\delta = O(\epsilon)$. When $\delta \ll \epsilon$, it degenerates to a one-phase problem where Φ_2 is no longer needed.

4. Reaction layer analysis: Slowly varying diffusivities. We start by considering the simplest case in which neither D_c nor D_h has any explicit dependence upon ϵ. As such they remain order 1, which we refer to as slowly varying. The reaction layer in these situations comprises a single region, which we describe here for the parameter range $\delta \leq \epsilon$, larger values of δ not being physically relevant for the carbonation problem. These slowly varying diffusivities provide a useful base case against which to compare the effects of more rapidly varying diffusivities in later sections 5 and 6.

4.1. Asymptotic regimes.

4.1.1. Case $\delta \leq \epsilon^{\frac{p+2}{p+1}}$. Fullest balance in the governing equations is obtained when $\delta = \lambda\epsilon^{\frac{p+2}{p+1}}$ with $\lambda = O(1)$. We introduce the scalings

$$x = s(t) + \epsilon^{\frac{2}{p+1}}\bar{x}, \qquad c = \epsilon^{\frac{2}{p+1}}\bar{c}, \qquad h = \bar{h}, \tag{27}$$

which preserve the CO_2 flux from outer 1, to obtain

$$\epsilon^{\frac{4}{p+1}}\mu\frac{\partial\bar{c}}{\partial t} - \epsilon^{\frac{2}{p+1}}\mu\dot{s}\frac{\partial\bar{c}}{\partial\bar{x}} - \frac{\partial}{\partial\bar{x}}\left(D_c\frac{\partial\bar{c}}{\partial\bar{x}}\right) = -\bar{c}^p\bar{h}^q, \tag{28}$$

$$\epsilon^{\frac{2}{p+1}}\frac{\partial\bar{h}}{\partial t} - \dot{s}\frac{\partial\bar{h}}{\partial\bar{x}} - \lambda^2\frac{\partial}{\partial\bar{x}}\left(D_h\frac{\partial\bar{h}}{\partial\bar{x}}\right) = -\bar{c}^p\bar{h}^q. \tag{29}$$

Posing

$$\bar{c} = \bar{c}_0 + o(1), \qquad \bar{h} = \bar{h}_0 + o(1), \tag{30}$$

with

$$D_c(c,h) \sim D_c(0,\bar{h}_0), \qquad D_h(c,h) \sim D_h(0,\bar{h}_0), \tag{31}$$

we obtain the leading order equations

$$\frac{\partial}{\partial\bar{x}}\left(D_c\frac{\partial\bar{c}_0}{\partial\bar{x}}\right) = \bar{c}_0^p\bar{h}_0^q, \qquad \dot{s}\frac{\partial\bar{h}_0}{\partial\bar{x}} + \lambda^2\frac{\partial}{\partial\bar{x}}\left(D_h\frac{\partial\bar{h}_0}{\partial\bar{x}}\right) = \bar{c}_0^p\bar{h}_0^q. \tag{32}$$

The matching conditions for outer 1 and 2 are

$$\text{as } \bar{x} \to -\infty, \qquad D_c\frac{\partial\bar{c}_0}{\partial\bar{x}} \to D_c\frac{\partial c_0(s^-,t)}{\partial x}, \quad \bar{h}_0 \to 0, \tag{33}$$

$$\text{as } \bar{x} \to +\infty, \qquad \bar{c}_0 \to 0, \quad \bar{h}_0 \to h_0(s^+,t), \quad \lambda^2 D_h\frac{\partial\bar{h}_0}{\partial\bar{x}} \to 0, \tag{34}$$

and necessarily $c_0(s^-,t) = 0$. Consequently, we have

$$\Phi_1 = 0, \tag{35}$$

while Φ_2 is not required. The above analysis also holds for $\delta \ll \epsilon^{\frac{p+2}{p+1}}$, where we can simply take the limit $\lambda \to 0$.

4.1.2. Case $\epsilon^{\frac{p+2}{p+1}} \ll \delta \ll \epsilon$. The scalings in this case are given by

$$x = s(t) + \delta\left(\frac{\epsilon}{\delta}\right)^p\bar{x}, \qquad c = \left(\frac{\delta}{\epsilon}\right)^2\bar{c}, \qquad h = \bar{h}, \tag{36}$$

to obtain

$$\delta^2\left(\frac{\epsilon}{\delta}\right)^{2p}\mu\frac{\partial\bar{c}}{\partial t} - \delta\left(\frac{\epsilon}{\delta}\right)^p\mu\dot{s}\frac{\partial\bar{c}}{\partial\bar{x}} - \frac{\partial}{\partial\bar{x}}\left(D_c\frac{\partial\bar{c}}{\partial\bar{x}}\right) = -\bar{c}^p\bar{h}^q, \tag{37}$$

$$\epsilon^2\left(\frac{\epsilon}{\delta}\right)^{2p}\frac{\partial\bar{h}}{\partial t} - \epsilon\left(\frac{\epsilon}{\delta}\right)^{p+1}\dot{s}\frac{\partial\bar{h}}{\partial\bar{x}} - \frac{\partial}{\partial\bar{x}}\left(D_h\frac{\partial\bar{h}}{\partial\bar{x}}\right) = -\bar{c}^p\bar{h}^q. \tag{38}$$

Posing

$$\bar{c} \sim \bar{c}_0 + \epsilon \left(\frac{\epsilon}{\delta}\right)^{p+1} \bar{c}_1, \qquad \bar{h} \sim \bar{h}_0 + \epsilon \left(\frac{\epsilon}{\delta}\right)^{p+1} \bar{h}_1, \tag{39}$$

we obtain the leading order equations

$$\frac{\partial}{\partial \bar{x}} \left(D_c \frac{\partial \bar{c}_0}{\partial \bar{x}} \right) = \bar{c}_0^p \bar{h}_0^q, \qquad \frac{\partial}{\partial \bar{x}} \left(D_h \frac{\partial \bar{h}_0}{\partial \bar{x}} \right) = \bar{c}_0^p \bar{h}_0^q, \tag{40}$$

while at first order we have (for brevity we record only the case in which both diffusivities are constant, additional terms from the expansion of the diffusivities being present when they are concentration dependent)

$$\frac{\partial}{\partial \bar{x}} \left(D_c \frac{\partial \bar{c}_1}{\partial \bar{x}} \right) = p \bar{c}_0^{p-1} \bar{h}_0^q \bar{c}_1 + q \bar{c}_0^p \bar{h}_0^{q-1} \bar{h}_1, \quad \dot{s} \frac{\partial \bar{h}_0}{\partial \bar{x}} + \frac{\partial}{\partial \bar{x}} \left(D_h \frac{\partial \bar{h}_1}{\partial \bar{x}} \right) = p \bar{c}_0^{p-1} \bar{h}_0^q \bar{c}_1 + q \bar{c}_0^p \bar{h}_0^{q-1} \bar{h}_1, \tag{41}$$

together with the matching conditions for outer 1 and 2 being

$$\text{as } \bar{x} \to -\infty, \qquad D_c \frac{\partial \bar{c}_0}{\partial \bar{x}} \to 0, \quad D_c \frac{\partial \bar{c}_1}{\partial \bar{x}} \to D_c \frac{\partial c_0(s^-, t)}{\partial x}, \quad \bar{h}_0 \to 0, \quad \bar{h}_1 \to 0, \tag{42}$$

$$\text{as } \bar{x} \to +\infty, \qquad \bar{c}_0 \to 0, \quad \bar{c}_1 \to 0, \quad \bar{h}_0 \to h_0(s^+, t), \quad D_h \frac{\partial \bar{h}_0}{\partial \bar{x}} \to 0, \quad D_h \frac{\partial \bar{h}_1}{\partial \bar{x}} \to D_h \frac{\partial h_0(s^+, t)}{\partial x}. \tag{43}$$

Necessarily $c_0(s,t) = 0$, and thus (35) holds with again Φ_2 not required. Here it is the first order terms which allow the fluxes to be matched with the outer regions.

4.1.3. Case $\delta = O(\epsilon)$. In this parameter case, an altogether quite different scenario takes place. First there is an initial period in which the reaction zone remains at the surface. This period may be termed stage I carbonation, using the terminology introduced for metal oxidation [10], where a similar situation occurs. During this stage, the hydroxide at the surface is depleted, the details of which are described in Appendix A. This stage ends at a finite time t_0 when the surface hydroxide concentration becomes small (i.e., zero at leading order). After this, stage II carbonation takes place where the reaction zone moves into the concrete, which we describe here.

Writing $\delta = \lambda\epsilon$ with $\lambda = O(1)$, the scalings are

$$x = s(t) + \epsilon^{\frac{2}{p+q+1}} \bar{x}, \qquad c = \epsilon^{\frac{2}{p+q+1}} \bar{c}, \qquad h = \epsilon^{\frac{2}{p+q+1}} \bar{h}, \tag{44}$$

giving

$$\epsilon^{\frac{4}{p+q+1}} \mu \frac{\partial \bar{c}}{\partial t} - \epsilon^{\frac{2}{p+q+1}} \mu \dot{s} \frac{\partial \bar{c}}{\partial \bar{x}} - \frac{\partial}{\partial \bar{x}} \left(D_c \frac{\partial \bar{c}}{\partial \bar{x}} \right) = -\bar{c}^p \bar{h}^q, \tag{45}$$

$$\epsilon^{\frac{4}{p+q+1}} \frac{\partial \bar{h}}{\partial t} - \epsilon^{\frac{2}{p+q+1}} \dot{s} \frac{\partial \bar{h}}{\partial \bar{x}} - \lambda^2 \frac{\partial}{\partial \bar{x}} \left(D_h \frac{\partial \bar{h}}{\partial \bar{x}} \right) = -\bar{c}^p \bar{h}^q. \tag{46}$$

Posing (30), we obtain the leading order equations

$$\frac{\partial}{\partial \bar{x}} \left(D_c \frac{\partial \bar{c}_0}{\partial \bar{x}} \right) = \bar{c}_0^p \bar{h}_0^q, \qquad \lambda^2 \frac{\partial}{\partial \bar{x}} \left(D_h \frac{\partial \bar{h}_0}{\partial \bar{x}} \right) = \bar{c}_0^p \bar{h}_0^q, \tag{47}$$

where $D_c(c,h) \sim D_c(0,0)$, $D_h(c,h) \sim D_h(0,0)$ are constants. The matching conditions for outer 1 and 2 are

$$\text{as } \bar{x} \to -\infty, \qquad D_c \frac{\partial \bar{c}_0}{\partial \bar{x}} \to D_c \frac{\partial c_0(s^-,t)}{\partial x}, \quad \bar{h}_0 \to 0, \tag{48}$$

$$\text{as } \bar{x} \to +\infty, \qquad \bar{c}_0 \to 0, \quad D_h \frac{\partial \bar{h}_0}{\partial \bar{x}} \to D_c \frac{\partial h_0(s^+,t)}{\partial x}. \tag{49}$$

Now, we have $c_0(s^-,t) = 0 = h_0(s^+,t)$ and consequently

$$\Phi_1 = 0 = \Phi_2. \tag{50}$$

4.2. Numerical results. Numerical solutions of the full model equations (9)–(13) are presented here for comparison with the asymptotics. The equations were implemented in the finite element package COMSOL Multiphysics, using the general-form PDE mode and a mesh of 400 quadratic Lagrange elements (1602 degrees of freedom). The time dependent (backward difference formula) solver had error tolerances abs tol $= 10^{-6}$, rel tol $= 10^{-3}$. For all numerical simulations we take initial data and parameter values as

$$h_i = 1, c_i = 0 \text{ for } 0 \le x \le 1, \quad \mu = 10^{-3}, \quad H = 10^4, \quad p = q = 1. \tag{51}$$

Figure 3 shows numerical solutions for the case $D_c = D_h = 1$ in the parameter regime $\epsilon = 10^{-3}$. Four selected values of δ have been chosen, covering the asymptotic regimes presented in section 4.1. The large value of the dimensionless mass transfer coefficient H effectively reduces the Robin condition to a Dirichlet one for c at the external interface $x = 0$. The no-flux condition for the hydroxide h at both fixed boundaries is always satisfied. There is a clear marked change in behavior between the case $\delta < \epsilon$, shown in (a)–(c), and $\delta = \epsilon$, shown in (d). The hydroxide profile falls to zero at the reaction front in (d) with noticeable diffusion ahead, in contrast to (a)–(c), where it is unity at the front and falls to zero within the reaction zone. Moreover, the rates at which the fronts move vary, with a time delay apparent in (d) compared to (a)–(c). This supports the stage I carbonation regime that is postulated to take place when $\delta = \epsilon$, in which the reaction zone remains at the surface for finite time as the hydroxide concentration falls. The reaction zone starts moving into the concrete once the hydroxide at the surface has been depleted.

4.3. Sharp-interface model summary. In the case $\delta \ll \epsilon$ we obtain the one-phase problem

$$\text{in } 0 < x < s(t),\ t > 0, \quad \mu \frac{\partial c_0}{\partial t} = \frac{\partial}{\partial x}\left(D_{c_0} \frac{\partial c_0}{\partial x} \right), \tag{52}$$

$$\text{on } x = 0, \qquad -D_{c_0} \frac{\partial c_0}{\partial x} = H(1 - c_0), \tag{53}$$

$$\text{on } x = s(t), \qquad c_0 = 0, \quad -D_{c_0} \frac{\partial c_0}{\partial x} = \dot{s} h_i(s), \tag{54}$$

$$\text{at } t = 0, \qquad c = c_i \text{ for } 0 \le x \le s_i, \quad s = s_i, \tag{55}$$

with $h_0 = h_i$ for $s(t) \le x < 1$.

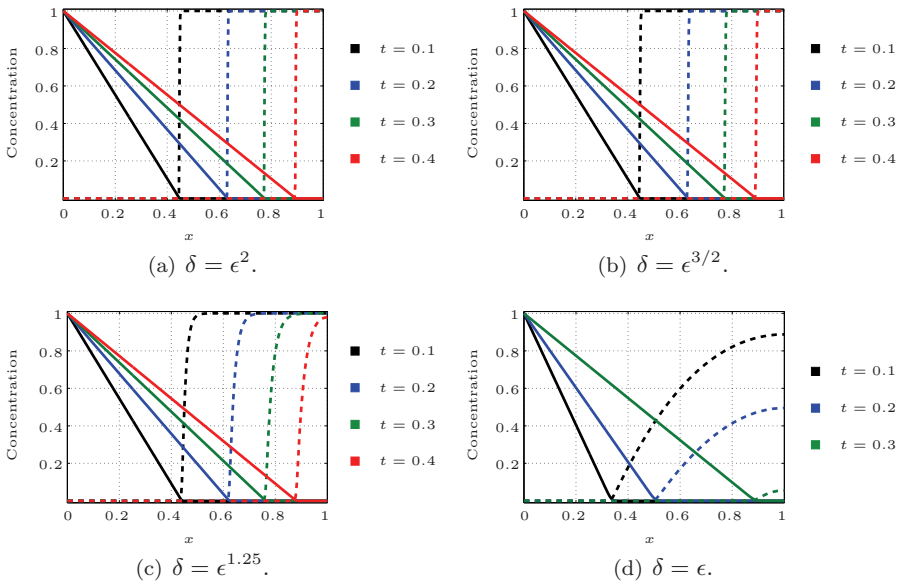

(a) $\delta = \epsilon^2$. (b) $\delta = \epsilon^{3/2}$.

(c) $\delta = \epsilon^{1.25}$. (d) $\delta = \epsilon$.

FIG. 3. *Numerical results for slowly varying diffusivities. The parameter values are* $\epsilon = 10^{-3}$, $p = q = 1$, $\mu = 10^{-3}$, $H = 10^4$, *and selected* δ *as stated in* (a)–(d). *The solid lines refer to the concentrations of carbon dioxide* c, *while the dotted lines are the concentrations of calcium hydroxide* h *at the shown times.*

In the case $\delta = \lambda\epsilon$ we obtain the two-phase problem

$$\text{(56)} \qquad \text{in } 0 < x < s(t),\ t > 0, \quad \mu \frac{\partial c_0}{\partial t} = \frac{\partial}{\partial x}\left(D_{c_0}\frac{\partial c_0}{\partial x}\right),$$

$$\text{(57)} \qquad \text{in } s(t) < x < 1,\ t > 0, \quad \frac{\partial h_0}{\partial t} = \lambda^2 \frac{\partial}{\partial x}\left(D_{h_0}\frac{\partial h_0}{\partial x}\right),$$

$$\text{(58)} \qquad \text{on } x = 0, \quad -D_{c_0}\frac{\partial c_0}{\partial x} = H(1 - c_0),$$

$$\text{(59)} \qquad \text{on } x = 1, \quad D_{h_0}\frac{\partial h_0}{\partial x} = 0,$$

$$\text{(60)} \qquad \text{on } x = s(t), \quad c_0 = 0, \quad h_0 = 0, \quad -D_{c_0}\frac{\partial c_0}{\partial x} = \lambda D_{h_0}\frac{\partial h_0}{\partial x},$$

$$\text{(61)} \qquad \text{at } t = t_0, \quad c_0 = C_i \text{ for } 0 \le x \le s_i,$$
$$h_0 = H_i \text{ for } s_i \le x \le 1, \quad s = s_i.$$

Here t_0 is the end of the time at which the reaction zone remains at the outer surface and after which it begins to ingress into the concrete. C_i, H_i denote the resulting concentration profiles at this time, which differ from their initial values c_i, h_i, respectively.

5. Reaction layer analysis: A single rapidly varying diffusivity. Here we consider the carbon dioxide diffusivity to depend on ϵ as well as the hydroxide concentration; i.e., $D_c = D_c(c, h; \epsilon)$. The hydroxide remains slowly varying; i.e.,

$D_h = O(1)$. The properties required for this diffusivity are

$$D_c = \begin{cases} O(\epsilon^2) & \text{for } h = O(1), h > 0, \\ O(1) & \text{for } h = o(1), h > 0. \end{cases} \tag{62}$$

While the functional form is not important, for definiteness we may consider a hydroxide-only dependent diffusivity $D_c(h;\epsilon)$ in the Arrhenius form

$$D_c = 1 - \exp\left(-\frac{\nu_1 \epsilon^2}{h^q}\right), \tag{63}$$

where ν_1 is a positive constant and $D_c(0;\epsilon) = 1$. (A more general power of h could be considered, with the below analysis needing only slight modification with the consideration of further terms in the expansions in the inner inner regions.)

5.1. Asymptotic regimes.

5.1.1. Case $\delta \leq \epsilon^2$. We write $\delta = \lambda\epsilon^2$ with $\lambda = O(1)$. The scalings for the inner inner region are

$$x = s(t) + \epsilon^2 \bar{x}, \qquad c = \bar{c}, \qquad h = \bar{h}, \qquad D_c = \epsilon^2 \bar{D}_c, \tag{64}$$

which give

$$\epsilon^2 \mu \frac{\partial \bar{c}}{\partial t} - \mu \dot{s} \frac{\partial \bar{c}}{\partial \bar{x}} - \frac{\partial}{\partial \bar{x}}\left(\bar{D}_c \frac{\partial \bar{c}}{\partial \bar{x}}\right) = -\bar{c}^p \bar{h}^q, \tag{65}$$

$$\epsilon^2 \frac{\partial \bar{h}}{\partial t} - \dot{s} \frac{\partial \bar{h}}{\partial \bar{x}} - \lambda^2 \frac{\partial}{\partial \bar{x}}\left(D_h \frac{\partial \bar{h}}{\partial \bar{x}}\right) = -\bar{c}^p \bar{h}^q. \tag{66}$$

Posing (30), we obtain at leading order

$$\mu \dot{s} \frac{\partial \bar{c}_0}{\partial \bar{x}} + \frac{\partial}{\partial \bar{x}}\left(\bar{D}_c \frac{\partial \bar{c}_0}{\partial \bar{x}}\right) = \bar{c}_0^p \bar{h}_0^q, \qquad \dot{s} \frac{\partial \bar{h}_0}{\partial \bar{x}} + \lambda^2 \frac{\partial}{\partial \bar{x}}\left(D_h \frac{\partial \bar{h}_0}{\partial \bar{x}}\right) = \bar{c}_0^p \bar{h}_0^q, \tag{67}$$

together with the matching conditions

$$\text{as } \bar{x} \to -\infty, \qquad \bar{c}_0 \to c_0(s^-, t), \quad \bar{D}_c \frac{\partial \bar{c}_0}{\partial \bar{x}} \to D_c \frac{\partial c_0(s^-, t)}{\partial x}, \quad \bar{h}_0 \to 0, \tag{68}$$

$$\text{as } \bar{x} \to +\infty, \qquad \bar{c}_0 \to 0, \quad \bar{h}_0 \to h_0(s^+, t), \quad \lambda^2 D_h \frac{\partial \bar{h}_0}{\partial \bar{x}} \to 0. \tag{69}$$

An additional region is required to facilitate the matching with outer 1 and explain (68), due to the order-of-magnitude change in the carbon dioxide diffusivity. We denote this region as inner 1, the scalings for which are

$$x = s(t) + \epsilon^{\frac{2}{q}} \hat{x}, \qquad c = \hat{c}, \qquad h = \epsilon^{\frac{2}{q}} \hat{h}, \tag{70}$$

giving

$$\epsilon^{\frac{4}{q}} \mu \frac{\partial \hat{c}}{\partial t} - \epsilon^{\frac{2}{q}} \mu \dot{s} \frac{\partial \hat{c}}{\partial \hat{x}} - \frac{\partial}{\partial \hat{x}}\left(D_c \frac{\partial \hat{c}}{\partial \hat{x}}\right) = -\epsilon^{\frac{4}{q}} \hat{c}^p \hat{h}^q, \tag{71}$$

$$\epsilon^{\frac{2}{q}} \frac{\partial \hat{h}}{\partial t} - \dot{s} \frac{\partial \hat{h}}{\partial \hat{x}} - \lambda^2 \epsilon^{\frac{2(q-1)}{q}} \frac{\partial}{\partial \hat{x}}\left(D_h \frac{\partial \hat{h}}{\partial \hat{x}}\right) = -\hat{c}^p \hat{h}^q. \tag{72}$$

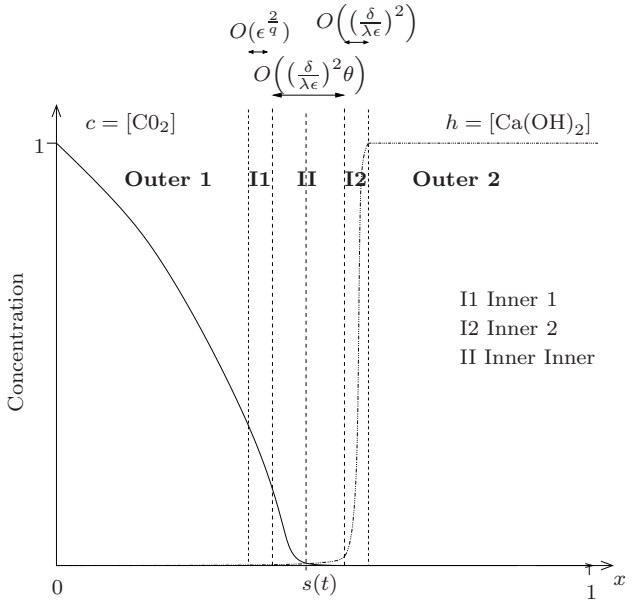

FIG. 4. *Schematic summary of the asymptotic regions for a rapidly varying CO_2 diffusivity in the parameter case $\epsilon^2 \ll \delta \ll \epsilon$. The reaction layer lies between outer regions outer 1 ($0 < x < s(t)$) and outer 2 ($s(t) < x < 1$). It is composed of three regions: an inner inner region (II) with $\theta = (\frac{\lambda\epsilon^2}{\delta})^{2/(1+q)}$, together with inners 1 (I1) and 2 (I2). The inners 1 and 2 facilitate the matching of the inner inner region with the two outers. The case shown is for $q > 1$ and $\delta \le \delta_{CR}$ with $\delta_{CR} = O(\epsilon^{(1+q)/q})$. Minor modifications are needed to inner 1 for the cases $q \le 1$ and $\delta > \delta_{CR}$.*

We restrict ourselves to the parameter case $q > 1$; the analysis needs a slight modification for $0 \le q \le 1$, which is described in Appendix B. Posing

$$\hat{c} \sim \hat{c}_0 + \epsilon^{\frac{2}{q}}\hat{c}_1, \qquad \hat{h} \sim \hat{h}_0, \tag{73}$$

we obtain

$$\frac{\partial}{\partial\hat{x}}\left(D_c\frac{\partial\hat{c}_0}{\partial\hat{x}}\right) = 0, \qquad \mu\dot{s}\frac{\partial\hat{c}_0}{\partial\hat{x}} + \frac{\partial}{\partial\hat{x}}\left(D_c\frac{\partial\hat{c}_1}{\partial\hat{x}}\right) = 0, \qquad \dot{s}\frac{\partial\hat{h}_0}{\partial\hat{x}} = \hat{c}_0^p\hat{h}_0^q. \tag{74}$$

After matching to outer 1 and the inner inner, we have

$$\hat{c}_0 = c_0(s^-,t) = \Phi_1, \quad D_c\frac{\partial\hat{c}_1}{\partial\hat{x}} = D_c\frac{\partial c_0(s^-,t)}{\partial x} = \lim_{\bar{x}\to-\infty}\bar{D}_c\frac{\partial\bar{c}_0}{\partial\bar{x}}, \tag{75}$$
$$\hat{h}_0 = \left(-\frac{(q-1)}{\dot{s}}c_0(s,t)^p\hat{x}\right)^{\frac{-1}{q-1}}.$$

5.1.2. Case $\epsilon^2 \ll \delta \ll \epsilon$. This case is more involved, where the reaction zone splits into three regions. In progressing from outer 2 to outer 1, we label the regions as inner 2, inner inner, and finally inner 1 as summarized in Figure 4.

The scalings for the inner 2 region are given by

$$x = s(t) + \left(\frac{\delta}{\lambda\epsilon}\right)^2\hat{x}, \qquad c = 0, \qquad h = \hat{h}, \qquad D_c = \epsilon^2\hat{D}_c, \tag{76}$$

where $\lambda = O(1)$ is introduced for convenience and c is actually exponentially small in ϵ if $p \geq 1$. The governing equation for the hydroxide at leading order in $\hat{x} > 0$ is

$$\dot{s}\frac{\partial \hat{h}_0}{\partial \hat{x}} + \lambda^2 \frac{\partial}{\partial \hat{x}}\left(D_h \frac{\partial \hat{h}_0}{\partial \hat{x}}\right) = 0, \tag{77}$$

together with the outer 2 matching conditions,

$$\text{as } \hat{x} \to +\infty, \qquad \hat{h}_0 \to h_0(s^+, t), \quad \frac{\partial \hat{h}_0}{\partial \hat{x}} \to 0. \tag{78}$$

Thus

$$\lambda^2 D_h \frac{\partial \hat{h}_0}{\partial \hat{x}} = \dot{s}(h_0(s^+, t) - \hat{h}),$$

and for matching with the inner inner we have the behavior

$$\text{as } \hat{x} \to 0^+, \qquad \hat{h}_0 \to 0, \quad \lambda^2 D_h \frac{\partial \hat{h}_0}{\partial \hat{x}} \to \dot{s} h_0(s^+, t). \tag{79}$$

In the case D_h a constant, we have the simple explicit solution,

$$\hat{h}_0 = h_0(s^+, t)\left(1 - \exp\left(-\frac{\dot{s}}{\lambda^2 D_h}\hat{x}\right)\right).$$

For the inner inner region, we adopt the scalings

$$x = s(t) + \left(\frac{\delta}{\lambda\epsilon}\right)^2 \theta \bar{x}, \qquad c = \bar{c}, \qquad h = \theta \bar{h}, \qquad D_c = \frac{\epsilon^2}{\theta^q}\bar{D}_c, \tag{80}$$

where

$$\theta = \left(\frac{\lambda \epsilon^2}{\delta}\right)^{\frac{2}{1+q}} \ll 1. \tag{81}$$

The governing equations are now

$$\left(\frac{\delta}{\lambda\epsilon}\right)^2 \theta\mu \frac{\partial \bar{c}}{\partial t} - \mu \dot{s}\frac{\partial \bar{c}}{\partial \bar{x}} - \frac{\partial}{\partial \bar{x}}\left(\bar{D}_c \frac{\partial \bar{c}}{\partial \bar{x}}\right) = -\bar{c}^p \bar{h}^q, \tag{82}$$

$$\left(\frac{\delta}{\lambda\epsilon}\right)^2 \theta^2 \frac{\partial \bar{h}}{\partial t} - \theta \dot{s}\frac{\partial \bar{h}}{\partial \bar{x}} - \lambda^2 \frac{\partial}{\partial \bar{x}}\left(D_h \frac{\partial \bar{h}}{\partial \bar{x}}\right) = -\bar{c}^p \bar{h}^q. \tag{83}$$

At leading order we have

$$\mu \dot{s}\frac{\partial \bar{c}_0}{\partial \bar{x}} + \frac{\partial}{\partial \bar{x}}\left(\bar{D}_c \frac{\partial \bar{c}_0}{\partial \bar{x}}\right) = \bar{c}_0^p \bar{h}_0^q, \qquad \lambda^2 \frac{\partial}{\partial \bar{x}}\left(D_h \frac{\partial \bar{h}_0}{\partial \bar{x}}\right) = \bar{c}_0^p \bar{h}_0^q, \tag{84}$$

together with the inner 2 matching conditions,

$$\text{as } \bar{x} \to +\infty, \qquad \bar{c}_0 \to 0, \quad \bar{D}_c \frac{\partial \bar{c}_0}{\partial \bar{x}} \to 0, \quad \bar{D}_h \frac{\partial \bar{h}_0}{\partial \bar{x}} \to \bar{D}_h \frac{\partial \hat{h}_0(0^+, t)}{\partial \hat{x}}, \tag{85}$$

and the inner 1 matching behavior

$$\text{as } \bar{x} \to -\infty, \qquad \bar{c}_0 \to \hat{c}_0(0^-,t), \quad \bar{D}_c \frac{\partial \bar{c}_0}{\partial \bar{x}} \to \hat{D}_c \frac{\partial \hat{c}_0(0^-,t)}{\partial \hat{x}}, \quad \bar{h}_0 \to 0. \tag{86}$$

To allow matching between the inner inner and outer 1, an inner 1 region is required. The scalings are determined by the size of δ relative to a critical value $\delta_{cr} = O(\epsilon^{(1+q)/q})$ and the value of q. We consider first the case $q > 1$, for which $\epsilon^2 \ll \delta_{cr} \ll \epsilon$. For $\delta < \delta_{cr}$ the scalings (70) apply, as does the subsequent analysis culminating in (75). This also pertains when $\delta = \delta_{cr}$, with the modification of the diffusion term entering the leading order hydroxide equation. For $\delta > \delta_{cr}$, the scalings need adjusting to

$$x = s(t) + \left(\frac{\delta}{\lambda\epsilon}\right)\epsilon^{\frac{1}{q}}\hat{x}, \qquad c = \hat{c}, \qquad h = \epsilon^{\frac{2}{q}}\hat{h}, \tag{87}$$

which give

$$\left(\frac{\delta}{\lambda\epsilon}\right)^2 \epsilon^{\frac{2}{q}}\mu\frac{\partial \hat{c}}{\partial t} - \left(\frac{\delta}{\lambda\epsilon}\right)\epsilon^{\frac{1}{q}}\mu\dot{s}\frac{\partial \hat{c}}{\partial \hat{x}} - \frac{\partial}{\partial \hat{x}}\left(D_c\frac{\partial \hat{c}}{\partial \hat{x}}\right) = -\left(\frac{\delta}{\lambda\epsilon}\right)^2 \epsilon^{\frac{2}{q}}\hat{c}^p\hat{h}^q, \tag{88}$$

$$\epsilon^{\frac{2}{q}}\frac{\partial \hat{h}}{\partial t} - \left(\frac{\epsilon}{\lambda\delta}\right)\epsilon^{\frac{1}{q}}\dot{s}\frac{\partial \hat{h}}{\partial \hat{x}} - \frac{\partial}{\partial \hat{x}}\left(D_h\frac{\partial \hat{h}}{\partial \hat{x}}\right) = -\hat{c}^p\hat{h}^q. \tag{89}$$

Posing

$$\hat{c} \sim \hat{c}_0 + \left(\frac{\delta}{\epsilon}\right)\epsilon^{\frac{1}{q}}\hat{c}_1, \qquad \hat{h} \sim \hat{h}_0, \tag{90}$$

we obtain

$$\frac{\partial}{\partial \hat{x}}\left(D_c\frac{\partial \hat{c}_0}{\partial \hat{x}}\right) = 0, \qquad \mu\dot{s}\frac{\partial \hat{c}_0}{\partial \hat{x}} + \frac{\partial}{\partial \hat{x}}\left(D_c\frac{\partial \hat{c}_1}{\partial \hat{x}}\right) = 0, \qquad \lambda^2\frac{\partial}{\partial \hat{x}}\left(D_h\frac{\partial \hat{h}_0}{\partial \hat{x}}\right) = \hat{c}_0^p\hat{h}_0^q. \tag{91}$$

After matching to outer 1 and the inner inner, we again obtain (75) with, for $q > 1$,

$$\hat{h}_0 = \left(\frac{(q-1)^2 c_0(s,t)^p}{2(1+q)D_h}\hat{x}^2\right)^{\frac{-1}{(q-1)}} \tag{92}$$

in the case when D_h is independent of $\hat{x}$.

For the range $q \le 1$, we note that $\delta_{cr} \le \epsilon^2$, and so it is the regime just discussed that occurs with slight modification. Specifically, for $q = 1$ this inner 1 region is the same size as the inner inner, and so the spatial scaling in (87) is modified to

$$x = s(t) + \frac{\delta}{\lambda}(S(t) + \hat{x}). \tag{93}$$

We again obtain (74)–(75), but now with

$$\hat{h}_0 = \exp\left(\sigma(t)\hat{x}\right), \qquad S(t) \sim \frac{-2}{q(1+q)\sigma(t)}\log\left(\left(\frac{\lambda\epsilon}{\delta}\right)^q\frac{1}{\epsilon}\right), \tag{94}$$

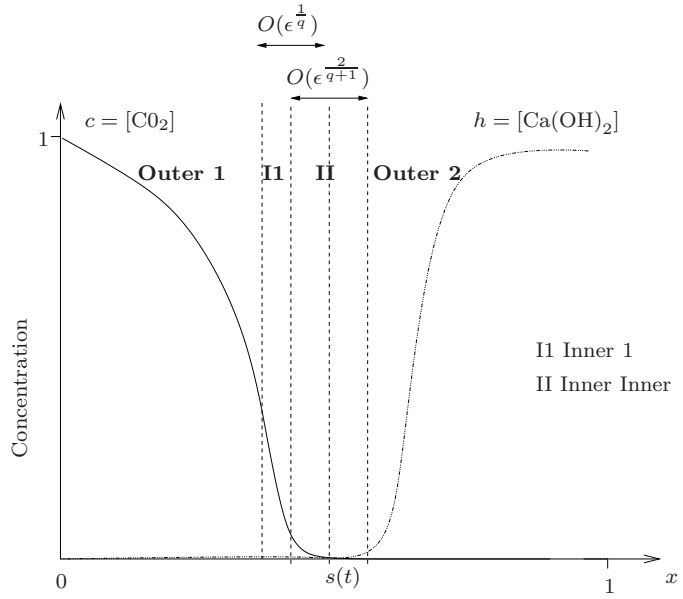

FIG. 5. *A schematic of the asymptotic regions in the case $\delta = O(\epsilon)$ of a single rapidly varying CO_2 diffusivity. The reaction zone is a two-layer structure, comprised of an inner inner region of width $O(\epsilon^{2/(q+1)})$, together with an inner 1 of width $O(\epsilon^{1/q})$. This latter transition region accommodates the change in the rapidly varying diffusivity, the situation $q > 1$ being depicted.*

where

$$\sigma(t) = \left(\frac{c_0(s^-, t)^p}{D_h} \right)^{\frac{1}{2}}.$$

When $q < 1$, the inner 1 region is narrower than the inner inner. We again have (75) and (92), where the latter solution is taken for $\hat{x} > 0$ and continued by zero for $\hat{x} < 0$. The inner inner region is now restricted to $\bar{x} > 0$ with the inner 1 matching conditions (75) occurring as $\bar{x} \to 0^+$.

5.1.3. Case $\delta = O(\epsilon)$. At the end of stage I carbonation (where the reaction zone remains at the outer surface), stage II carbonation takes place, in which the reaction zone moves into the concrete.

In this case the reaction zone comprises two regions, as shown in Figure 5. We have an inner inner region that matches the order 1 flux of hydroxide from the outer 2 region as well as allowing the CO_2 concentration to fall to $o(1)$. Again an inner 1 region is needed to accommodate the fall in CO_2 diffusivity, allowing matching between the inner inner and outer 1 regions. The details can be deduced from the previous subsection by setting $\delta = \lambda\epsilon$ with $\lambda = O(1)$. Consequently, for the inner inner region the scalings (80) apply with $\theta = \epsilon^{2/(1+q)}$ so that again we obtain (84) as the leading order equations. Since there is now no inner 2 region in this case, the matching conditions (85) apply to outer 2, with $\hat{h}_0$ being replaced with h_0. The inner 1 matching conditions (86) remain the same, as do the details for the inner 1 region as given by (87)–(94).

5.2. Numerical results. Here we present numerical simulations for a rapidly varying CO_2 diffusivity, using the scheme and data/parameter values specified in

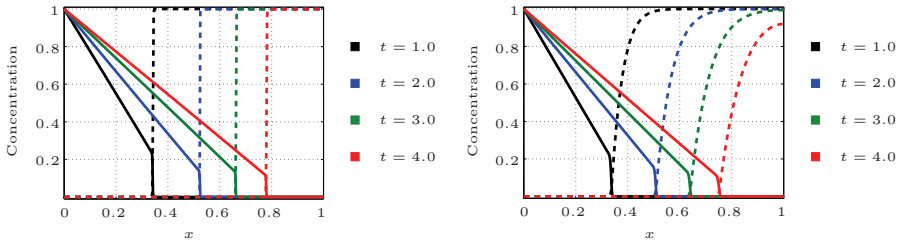

(a) $\delta = \epsilon^2$.

(b) $\delta = \epsilon^{3/2}$.

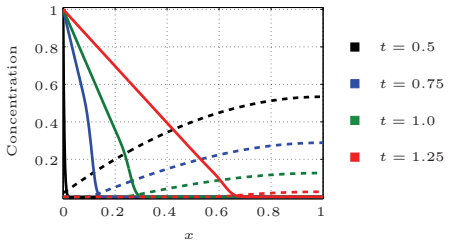

(c) $\delta = \epsilon$.

FIG. 6. *Numerical results for one rapidly varying diffusion coefficient D_c as defined in* (63) *for $\epsilon = 10^{-2}$, $p = q = 1$, $\mu = 10^{-3}$, and $H = 10^4$. The solid lines refer to the concentrations of carbon dioxide c, while the dotted lines are the concentrations of calcium hydroxide h.*

section 4.2. We found it necessary to use the following regularization for the diffusion coefficient (63):

$$D_c = 1 - \exp\left(-\frac{\nu_1 \epsilon^2}{(h^2 + \theta_1^2)^{\frac{q}{2}}}\right), \tag{95}$$

with $\theta_1 = 10^{-3}$. Although we don't present results for $p \neq 1$, $q \neq 1$, we found the following regularization of the reaction term useful in avoiding numerical difficulties:

$$r = c(c^2 + \theta_1^2)^{\frac{p-1}{2}} h(h^2 + \theta_1^2)^{\frac{q-1}{2}},$$

particularly for $p < 1$ or $q < 1$.

Figure 6 shows the numerical results for $\epsilon = 10^{-2}$. Three selected cases of δ are shown, covering the different asymptotic regimes noted in the previous section. Noteworthy features are the $O(1)$ concentrations of CO_2 at the reaction zone in all cases. Also the slower progress of the reaction zone compared to the corresponding situation in the slowly varying diffusivity case. Again the case $\delta = O(\epsilon)$ shown in Figure 6(c) gives different behavior to the case $\delta \ll \epsilon$, with the hydroxide concentration being small at the reaction zone front and stage I carbonation taking place initially.

5.3. Sharp-interface model summary. In the case $\delta \leq \epsilon^2$, we now obtain the one-phase problem (52)–(55) but with the more general moving-boundary condition

$$\text{on } x = s(t),\ c_0 = \Phi_1(\dot{s}), \quad -D_{c_0}\frac{\partial c_0}{\partial x} = \dot{s}(\mu c_0 + h_i(s)), \tag{96}$$

in place of (54). We remark that Φ_1 is determined by the solution of the inner inner problem

$$\mu\dot{s}\frac{\partial\bar{c}_0}{\partial\bar{x}}+\frac{\partial}{\partial\bar{x}}\left(\bar{D}_c\frac{\partial\bar{c}_0}{\partial\bar{x}}\right)=\bar{c}_0^p\bar{h}_0^q,\qquad \bar{D}_c\frac{\partial\bar{c}_0}{\partial\bar{x}}-\lambda^2D_h\frac{\partial\bar{h}_0}{\partial\bar{x}}=\dot{s}(\bar{h}_0-h_i(s)-\mu\bar{c}_0), \tag{97}$$

with

$$\text{as } \bar{x}\to+\infty,\qquad \bar{c}_0\to 0,\quad \bar{D}_c\frac{\partial\bar{c}_0}{\partial\bar{x}}\to 0,\quad \bar{h}_0\to h_i(s), \tag{98}$$

that satisfies

$$\text{as } \bar{x}\to-\infty,\qquad \bar{c}_0\to\Phi_1(\dot{s}),\quad \bar{h}_0\to 0,\quad D_h\frac{\partial\bar{h}_0}{\partial\bar{x}}\to 0. \tag{99}$$

For the functional form (63) we have $\bar{D}_c=\nu_1/\bar{h}_0^q$.

For $\epsilon^2\ll\delta\ll\epsilon$ we again have a one-phase model with moving-boundary condition (96), but now Φ_1 is determined by the solution of the inner inner 1 problem

$$\mu\dot{s}\frac{\partial\bar{c}_0}{\partial\bar{x}}+\frac{\partial}{\partial\bar{x}}\left(\bar{D}_c\frac{\partial\bar{c}_0}{\partial\bar{x}}\right)=\bar{c}_0^p\bar{h}_0^q,\qquad \bar{D}_c\frac{\partial\bar{c}_0}{\partial\bar{x}}-\lambda^2D_h\frac{\partial\bar{h}_0}{\partial\bar{x}}=-\dot{s}(h_i(s)+\mu\bar{c}_0), \tag{100}$$

with

$$\text{as } \bar{x}\to+\infty,\qquad \bar{c}_0\to 0,\quad \bar{D}_c\frac{\partial\bar{c}_0}{\partial\bar{x}}\to 0,\quad \lambda^2D_h\frac{\partial\bar{h}_0}{\partial\bar{x}}\to\dot{s}h_i(s), \tag{101}$$

$$\text{as } \bar{x}\to-\infty,\qquad \bar{c}_0\to\Phi_1(\dot{s}),\quad \bar{h}_0\to 0,\quad D_h\frac{\partial\bar{h}_0}{\partial\bar{x}}\to 0. \tag{102}$$

In the case $\delta=O(\epsilon)$, we now obtain the two-phase problem (56)–(61) but with the more general moving-boundary condition

$$\text{on } x=s(t),\qquad c_0=\Phi_1(\dot{s}),\quad -D_{c_0}\frac{\partial c_0}{\partial x}-\lambda^2D_{h_0}\frac{\partial h_0}{\partial x}=\dot{s}\mu c_0, \tag{103}$$

in place of (60). We remark that the outer 2 solution determines $\Phi_2=0$, while Φ_1 is determined by the solution of the inner inner problem

$$\mu\dot{s}\frac{\partial\bar{c}_0}{\partial\bar{x}}+\frac{\partial}{\partial\bar{x}}\left(\bar{D}_c\frac{\partial\bar{c}_0}{\partial\bar{x}}\right)=\bar{c}_0^p\bar{h}_0^q,\qquad \lambda^2\frac{\partial}{\partial\bar{x}}\left(D_h\frac{\partial\bar{h}_0}{\partial\bar{x}}\right)=\bar{c}_0^p\bar{h}_0^q, \tag{104}$$

with

$$\text{as } \bar{x}\to+\infty,\qquad \bar{c}_0\to 0,\quad \bar{D}_c\frac{\partial\bar{c}_0}{\partial\bar{x}}\to 0,\quad D_h\frac{\partial\bar{h}_0}{\partial\bar{x}}\to D_h\frac{\partial h_0(s^+,t)}{\partial x}, \tag{105}$$

$$\text{as } \bar{x}\to-\infty,\qquad \bar{c}_0\to\Phi_1(\dot{s}),\quad \bar{h}_0\to 0,\quad D_h\frac{\partial\bar{h}_0}{\partial\bar{x}}\to 0. \tag{106}$$

This formulation holds for the parameter range $q\geq 1$. For $q<1$, the boundary condition (106) is applied at $\bar{x}=0^+$, and the problem considered on the half-line $\bar{x}>0$.

6. Reaction layer analysis: Two rapidly varying diffusivities. We now consider the situation in which both the carbon dioxide and hydroxide diffusivities are rapidly varying. In addition to D_c as defined in section 5, we consider a hydroxide diffusivity $D_h = D_h(c;\epsilon)$ with the behavior

$$D_h = \begin{cases} O(\delta^2) & \text{for } c = O(1), c > 0, \\ O(1) & \text{for } c = o(1), c > 0, \end{cases} \tag{107}$$

and $D_h(0;\epsilon) = 1$. This maintains an $O(1)$ flux of hydroxide in the reaction zone. For definiteness, a specific functional form could be the Arrhenius type,

$$D_h = 1 - \exp\left(-\frac{\nu_2 \delta^2}{c^p}\right), \tag{108}$$

where ν_2 is a positive constant.

6.1. Asymptotic regimes.

6.1.1. Case $\delta = O(\epsilon)$. Writing $\delta = \lambda\epsilon$ with $\lambda = O(1)$, the scalings for the inner inner region are

$$x = s(t) + \epsilon^2 \bar{x}, \quad c = \bar{c}, \quad h = \bar{h}, \quad D_c = \epsilon^2 \bar{D}_c, \quad D_h = \left(\frac{\delta}{\lambda}\right)^2 \bar{D}_h, \tag{109}$$

which give

$$\epsilon^2 \mu \frac{\partial \bar{c}}{\partial t} - \mu \dot{s} \frac{\partial \bar{c}}{\partial \bar{x}} - \frac{\partial}{\partial \bar{x}}\left(\bar{D}_c \frac{\partial \bar{c}}{\partial \bar{x}}\right) = -\bar{c}^p \bar{h}^q, \tag{110}$$

$$\epsilon^2 \frac{\partial \bar{h}}{\partial t} - \dot{s} \frac{\partial \bar{h}}{\partial \bar{x}} - \left(\frac{\delta^2}{\lambda \epsilon^2}\right)^2 \frac{\partial}{\partial \bar{x}}\left(\bar{D}_h \frac{\partial \bar{h}}{\partial \bar{x}}\right) = -\bar{c}^p \bar{h}^q. \tag{111}$$

Posing (30), we obtain at leading order

$$\mu \dot{s} \frac{\partial \bar{c}_0}{\partial \bar{x}} + \frac{\partial}{\partial \bar{x}}\left(\bar{D}_c \frac{\partial \bar{c}_0}{\partial \bar{x}}\right) = \bar{c}_0^p \bar{h}_0^q, \qquad \dot{s} \frac{\partial \bar{h}_0}{\partial \bar{x}} + \lambda^2 \frac{\partial}{\partial \bar{x}}\left(\bar{D}_h \frac{\partial \bar{h}_0}{\partial \bar{x}}\right) = \bar{c}_0^p \bar{h}_0^q, \tag{112}$$

together with the matching conditions

$$\text{as } \bar{x} \to -\infty, \qquad \bar{D}_c \frac{\partial \bar{c}_0}{\partial \bar{x}} \to D_c \frac{\partial c_0(s^-,t)}{\partial x}, \quad \bar{h}_0 \to 0, \tag{113}$$

$$\text{as } \bar{x} \to +\infty, \qquad \bar{c}_0 \to 0, \quad \bar{D}_h \frac{\partial \bar{h}_0}{\partial \bar{x}} \to D_h \frac{\partial h_0(s^+,t)}{\partial x}. \tag{114}$$

Again additional regions are required to facilitate the matching with outer 1 and 2, due to the order-of-magnitude change in the diffusivities. As in the single rapidly varying diffusivity case in section 5.1 we require an inner 1 region, the scalings for which are

$$x = s(t) + \epsilon^{\frac{2}{q}} \hat{x}, \qquad c = \hat{c}, \qquad h = \epsilon^{\frac{2}{q}} \hat{h}, \qquad D_h = \left(\frac{\delta}{\lambda}\right)^2 \hat{D}_h, \tag{115}$$

giving (71)–(72), resulting in the same matching conditions (75) (with care taken to distinguish the cases $0 \le q < 1$, $q = 1$, and $q > 1$).

To facilitate the matching with outer 2, we consider an inner 2 region with the scalings

$$x = s(t) + \epsilon^2(S(t;\epsilon) + \hat{x}), \qquad c = \epsilon^{\frac{2}{p}}\hat{c}, \qquad h = \hat{h}, \qquad D_c = \epsilon^2\hat{D}_c, \tag{116}$$

where $S(t;\epsilon) \gg 1$. Thus we have

$$\epsilon^2\mu\frac{\partial\hat{c}}{\partial t} - \mu(\dot{s} + \epsilon^2\dot{S})\frac{\partial\hat{c}}{\partial\hat{x}} - \frac{\partial}{\partial\hat{x}}\left(\hat{D}_c\frac{\partial\hat{c}}{\partial\hat{x}}\right) = -\epsilon^{\frac{2(p-1)}{p}}\hat{c}^p\hat{h}^q, \tag{117}$$

$$\epsilon^4\frac{\partial\hat{h}}{\partial t} - \epsilon^2(\dot{s} + \epsilon^2\dot{S})\frac{\partial\hat{h}}{\partial\hat{x}} - \lambda^2\frac{\partial}{\partial\hat{x}}\left(D_h\frac{\partial\hat{h}}{\partial\hat{x}}\right) = -\epsilon^4\hat{c}^p\hat{h}^q. \tag{118}$$

We restrict ourselves first to the parameter range $p > 1$. Posing

$$\hat{c} \sim \hat{c}_0, \qquad \hat{h} \sim \hat{h}_0 + \epsilon^2\hat{h}_1, \tag{119}$$

we obtain

$$\frac{\partial}{\partial\hat{x}}\left(D_h\frac{\partial\hat{h}_0}{\partial\hat{x}}\right) = 0, \qquad \frac{\partial}{\partial\hat{x}}\left(D_h\frac{\partial\hat{h}_1}{\partial\hat{x}}\right) = 0, \qquad \mu\dot{s}\frac{\partial\hat{c}_0}{\partial\hat{x}} + \frac{\partial}{\partial\hat{x}}\left(\hat{D}_c\frac{\partial\hat{c}_0}{\partial\hat{x}}\right) = 0. \tag{120}$$

Thus we have

$$\hat{h}_0 = h_0(s^+,t) = \Phi_2, \quad D_h\frac{\partial\hat{h}_1}{\partial\hat{x}} = D_h\frac{\partial h_0(s^+,t)}{\partial x} = \lim_{\bar{x}\to+\infty}\bar{D}_h\frac{\partial\bar{h}_0}{\partial\bar{x}}, \quad \hat{c}_0 = \exp\left(-\frac{\mu\dot{s}\hat{x}}{\hat{D}_c}\right), \tag{121}$$

after matching to outer 2 and the inner inner regions, which also determines

$$S(t;\epsilon) \sim \frac{2\dot{s}\hat{D}_c}{p}\log(1/\epsilon) \qquad \text{as } \epsilon \to 0. \tag{122}$$

For $p = 1$, a minor modification of the above takes place with the leading order reaction term entering the equation for $\hat{c}_0$ in (120). For $0 < p < 1$, the inner inner solution for $\bar{c}_0$ vanishes at $\bar{x} = S(t)$, say, and we modify the spatial scaling in (116) to

$$x = s(t) + \epsilon^2\left(S(t) + \epsilon^{\frac{(1-p)}{p}}\hat{x}\right).$$

As a result the leading order equation for $\hat{c}$ becomes

$$\frac{\partial}{\partial\hat{x}}\left(\hat{D}_c\frac{\partial\hat{c}_0}{\partial\hat{x}}\right) = \hat{c}_0^p\hat{h}_0^q,$$

with $\hat{D}_c = \nu_1/h_0(s^+,t)^q$, which possesses the explicit solution

$$\hat{c}_0 = \begin{cases} \left(\frac{(1-p)^2h_0(s^+,t)^q}{2(1+p)\hat{D}_c}\hat{x}^2\right)^{\frac{1}{1-p}} & \text{for } \hat{x} < 0, \\ 0 & \text{for } \hat{x} > 0. \end{cases} \tag{123}$$

6.1.2. Case $\delta \ll \epsilon$. Only slight modification of the preceding analysis is required for this case. The inner inner region remains the same with the scalings (109), but now (112) becomes

$$\mu\dot{s}\frac{\partial \bar{c}_0}{\partial \bar{x}} + \frac{\partial}{\partial \bar{x}}\left(\bar{D}_c\frac{\partial \bar{c}_0}{\partial \bar{x}}\right) = \bar{c}_0^p\bar{h}_0^q, \qquad \dot{s}\frac{\partial \bar{h}_0}{\partial \bar{x}} = \bar{c}_0^p\bar{h}_0^q, \tag{124}$$

with the second condition in (114) replaced by

$$\text{as } \bar{x} \to +\infty, \qquad \bar{h}_0 \to h_0(s^+, t). \tag{125}$$

The inner 1 analysis with scalings (115) remains the same for $q > 1$, while for $q = 1$ the only change is omission of the hydroxide diffusion term which is subdominant. There is more of a change for $0 < q < 1$, where the spatial scaling and balance in the hydroxide equation now depend upon the size of δ relative to $\delta_{cr} = \epsilon^{(1+q)/2q}$. Specifically,

(i) for $\delta \le \delta_{cr}$, $x = s(t) + \epsilon^2\left(S(t) + \epsilon^{2(1-q)/q}\hat{x}\right)$, the dominant balance for the hydroxide equation being that in (74) for $\delta < \delta_{cr}$ and (177) in Appendix B when $\delta = \delta_{cr}$;

(ii) for $\delta_{cr} < \delta < \epsilon$, $x = s(t) + \epsilon^2\left(S(t) + \left(\frac{\delta}{\lambda\epsilon}\right)^2\epsilon^{(1-q)/q}\hat{x}\right)$, the dominant balance for the hydroxide equation being (183) in Appendix B.

The inner 2 analysis remains unchanged (allowing for modified scalings) for $\epsilon^2 \ll \delta \ll \epsilon$, where $\lambda = \delta/\epsilon \ll 1$ in (118). For $\delta = \epsilon^2$, the convection term balances the diffusion term in the hydroxide equation (118). However, the leading order behaviors in (121) remain unchanged. For $\delta \ll \epsilon^2$, the hydroxide convection and diffusion terms balance in a thin region of size $\hat{x} = (\delta/\epsilon^2)^2$ centered at $S(t)$, which allows the required matching to outer 2. These statements apply for $p \ge 1$, more care being needed for $p < 1$.

6.2. Numerical results. We implement the scheme as in the previous numerical sections 4.2 and 5.2, using the same initial data and parameter values. A regularization analogous to (95) is adopted for the hydroxide diffusivity (108).

Figure 7 shows the numerical results for $\epsilon = 10^{-2}$ and three selected values of δ. Compared to the single rapidly varying CO_2 diffusivity, the addition of a rapidly varying hydroxide diffusivity further slows down the progress of the reaction zone. The most significant change occurs in the $\delta = \epsilon$ regime, where now the hydroxide concentration is $O(1)$ in the reaction zone and no longer small as for the slowly varying and single rapidly varying CO_2 cases in sections 4.2 and 5.2. Stage I carbonation no longer takes place in this case.

6.3. Sharp-interface model summary. In the case $\delta = \epsilon$, we obtain the two-phase problem (56)–(61) but with the more general moving-boundary condition

$$\text{on } x = s(t), \quad c_0 = \Phi_1(\dot{s}), \quad h_0 = \Phi_2(\dot{s}), \quad -D_{c_0}\frac{\partial c_0}{\partial x} - \lambda^2 D_{h_0}\frac{\partial h_0}{\partial x} = \dot{s}(\mu c_0 + h_0), \tag{126}$$

in place of (60). The solution of the inner inner problem

$$\mu\dot{s}\frac{\partial \bar{c}_0}{\partial \bar{x}} + \frac{\partial}{\partial \bar{x}}\left(\bar{D}_c\frac{\partial \bar{c}_0}{\partial \bar{x}}\right) = \bar{c}_0^p\bar{h}_0^q, \qquad \dot{s}\frac{\partial \bar{h}_0}{\partial \bar{x}} + \frac{\partial}{\partial \bar{x}}\left(\bar{D}_h\frac{\partial \bar{h}_0}{\partial \bar{x}}\right) = \bar{c}_0^p\bar{h}_0^q, \tag{127}$$

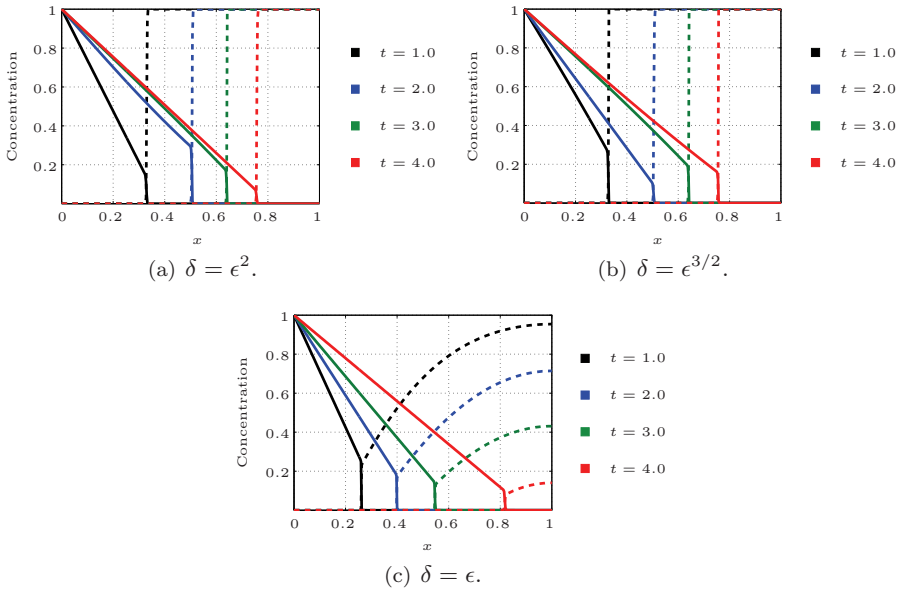

(a) $\delta = \epsilon^2$. (b) $\delta = \epsilon^{3/2}$.

(c) $\delta = \epsilon$.

FIG. 7. *Numerical results for two rapidly varying diffusivities. The parameter values are* $\epsilon = 10^{-2}$, $p = q = 1$, $\mu = 10^{-3}$, *and* $H = 10^4$. *The solid lines refer to the concentrations of carbon dioxide* c, *while the dotted lines are the concentrations of calcium hydroxide* h.

with

$$\text{as } \bar{x} \to +\infty, \qquad \bar{c}_0 \to 0, \quad \bar{D}_c \frac{\partial \bar{c}_0}{\partial \bar{x}} \to 0, \tag{128}$$

$$\text{as } \bar{x} \to -\infty, \qquad \bar{h}_0 \to 0, \quad \bar{D}_h \frac{\partial \bar{h}_0}{\partial \bar{x}} \to 0, \tag{129}$$

determines Φ_1, Φ_2 via

$$\Phi_1(\dot{s}) = \lim_{\bar{x} \to -\infty} \bar{c}_0, \qquad \Phi_2(\dot{s}) = \lim_{\bar{x} \to +\infty} \bar{h}_0. \tag{130}$$

In the case $\delta \ll \epsilon$, we have the one-phase problem (52)–(55) with (54) replaced by

$$\text{on } x = s(t), \quad c_0 = \Phi_1(\dot{s}), \quad -D_{c_0} \frac{\partial c_0}{\partial x} = \dot{s}(\mu c_0 + h_i(s)), \tag{131}$$

where Φ_1 is determined by the solution of the inner inner problem

$$\mu \dot{s} \frac{\partial \bar{c}_0}{\partial \bar{x}} + \frac{\partial}{\partial \bar{x}} \left(\bar{D}_c \frac{\partial \bar{c}_0}{\partial \bar{x}} \right) = \bar{c}_0^p \bar{h}_0^q, \qquad \bar{D}_c \frac{\partial \bar{c}_0}{\partial \bar{x}} = \dot{s}(\bar{h}_0 - h_i(s) - \mu \bar{c}_0), \tag{132}$$

with

$$\text{as } \bar{x} \to +\infty, \qquad \bar{c}_0 \to 0, \quad \bar{D}_c \frac{\partial \bar{c}_0}{\partial \bar{x}} \to 0, \quad \bar{h}_0 \to h_i(s), \tag{133}$$

$$\text{as } \bar{x} \to -\infty, \qquad \bar{c}_0 \to \Phi_1(\dot{s}), \quad \bar{h}_0 \to 0. \tag{134}$$

For the functional forms (63) and (108) we have $\bar{D}_c = \nu_1 / \bar{h}_0^q$, $\bar{D}_h = \nu_2 / \bar{c}_0^p$.

7. The derived generalized Stefan problems.

7.1. The one-phase problem. In the case $\delta \ll \epsilon$ we obtain the one-phase problem

$$\text{in } 0 < x < s(t),\ t > 0, \quad \mu \frac{\partial c_0}{\partial t} = \frac{\partial}{\partial x}\left(D_{c_0} \frac{\partial c_0}{\partial x} \right), \tag{135}$$

$$\text{on } x = 0, \qquad -D_{c_0} \frac{\partial c_0}{\partial x} = H(1 - c_0), \tag{136}$$

$$\text{on } x = s(t), \qquad c_0 = \Phi_1(\dot{s}), \quad -D_{c_0} \frac{\partial c_0}{\partial x} = \dot{s}(\mu c_0 + h_i(s)), \tag{137}$$

$$\text{at } t = 0, \qquad c = c_i \text{ for } 0 \le x \le s_i, \quad s = s_i, \tag{138}$$

with $h_0 = h_i$ for $s(t) \le x < 1$. For a slowly varying CO_2 diffusivity, the analysis of section 4 implies $\Phi_1 = 0$, while for a rapidly varying CO_2 diffusivity, Φ_1 is given as the solution of the problem (97)–(99) or (100)–(102), depending upon the size of δ relative to ϵ^2, or (132)–(134) if the hydroxide diffusivity varies rapidly as well.

The parameter $1/\mu$ represents the Stefan number, the time scaling $t = \mu\tau$ seeing it arise in the Stefan condition in (137) for its more common occurrence. The asymptotics of this problem for power law forms of $\Phi_1 = \dot{s}^n$ are described in [9, 11]. Relevant to the concrete situation is the large Stefan number limit $\mu \to 0$. In this limit, the problem becomes quasi-steady due to the now disparate time scales of diffusion and reaction. This quasi-steady problem holds after an initial transient regime $t = O(\mu)$ in which the interface is stationary at leading order. An explicit solution for the quasi-steady problem $t > O(\mu)$ when $D_{c_0} \equiv 1$ is

$$c_0 = \Phi_1 + \frac{(1 - \Phi_1)(s - x)}{\left(\frac{1}{H} + s\right)}, \tag{139}$$

with the interface $s(t)$ determined by the solution of

$$h_i(s)\left(\frac{1}{H} + s\right)\dot{s} + \Phi_1(\dot{s}) = 1, \qquad s(0) = s_i. \tag{140}$$

7.2. The two-phase problem. In the case $\delta = \lambda\epsilon$ we obtain the two-phase problem

$$\text{in } 0 < x < s(t),\ t > 0, \quad \mu \frac{\partial c_0}{\partial t} = \frac{\partial}{\partial x}\left(D_{c_0} \frac{\partial c_0}{\partial x} \right), \tag{141}$$

$$\text{in } s(t) < x < 1,\ t > 0, \quad \frac{\partial h_0}{\partial t} = \lambda^2 \frac{\partial}{\partial x}\left(D_{h_0} \frac{\partial h_0}{\partial x} \right), \tag{142}$$

$$\text{on } x = 0, \qquad -D_{c_0} \frac{\partial c_0}{\partial x} = H(1 - c_0), \tag{143}$$

$$\text{on } x = 1, \qquad D_{h_0} \frac{\partial h_0}{\partial x} = 0, \tag{144}$$

$$\text{on } x = s(t), \qquad c_0 = \Phi_1(\dot{s}), \quad h_0 = \Phi_2(\dot{s}), \tag{145}$$

$$-D_{c_0} \frac{\partial c_0}{\partial x} - \lambda^2 D_{h_0} \frac{\partial h_0}{\partial x} = \dot{s}\left(\mu c_0 + h_0\right),$$

$$\text{at } t = t_0, \qquad c_0 = C_i \text{ for } 0 \le x \le s_i, \tag{146}$$

$$h_0 = H_i \text{ for } s_i \le x \le 1, \quad s = s_i.$$

Here t_0 is the end of the time at which the reaction zone remains at the outer surface and after which it begins to ingress into the concrete. C_i, H_i denote the resulting concentration profiles at this time, which differ from their initial values c_i, h_i, respectively. For slowly varying CO_2 and $Ca(OH)_2$ diffusivities, the analysis of section 4 implies $\Phi_1 = 0 = \Phi_2$. For a single rapidly varying CO_2 diffusivity, Φ_1 is given as the solution of the problem (104)–(106) with $\Phi_2 = 0$. In both these situations there is a stage I carbonation period where the $Ca(OH)_2$ concentration in the initial reaction zone at the surface falls to zero. When both diffusivities are rapidly varying, then Φ_1, Φ_2 are determined by (127)–(129), there not being a stage I carbonation period in this case.

In the quasi-steady CO_2 limit $\mu \to 0$, we again have solution (139) in the case $D_{c_0} \equiv 1$. This gives the non-standard Stefan problem for the $Ca(OH)_2$ as

$$\text{(147)} \qquad \text{in } s(t) < x < 1,\ t > 0, \quad \frac{\partial h_0}{\partial t} = \lambda^2 \frac{\partial}{\partial x}\left(D_{h_0} \frac{\partial h_0}{\partial x} \right),$$

$$\text{(148)} \qquad \text{on } x = 1, \qquad D_{h_0} \frac{\partial h_0}{\partial x} = 0,$$

$$\text{(149)} \qquad \text{on } x = s(t), \qquad \begin{cases} h_0 = \Phi_2(\dot{s}), \\ \lambda^2 D_{h_0} \frac{\partial h_0}{\partial x} = \frac{1}{\left(\frac{1}{H}+s\right)} - \frac{\Phi_1(\dot{s})}{\left(\frac{1}{H}+s\right)} - \dot{s}\Phi_2(\dot{s}), \end{cases}$$

$$\text{(150)} \qquad \text{at } t = t_0, \qquad h_0 = H_i \text{ for } s_i \le x \le 1, \quad s = s_i.$$

This problem in the slowly varying diffusivity case when $\Phi_1 = 0 = \Phi_2$ has been considered by [15] in the context of binary alloy oxidation. However, the more general statement has not received attention.

8. Discussion. A set of reaction-diffusion equations representing the concrete carbonation process has been analyzed in the limit of fast reaction–slow diffusion. Different sharp-interface models in the form of generalized Stefan problems are derived, depending upon the properties of the diffusivities (of the two main species CO_2 and $Ca(OH)_2$) as well as the size of the relative transport parameter $\delta^2/\epsilon^2 = D_h^0 h^0 / D_c^0 C^* \le O(1)$. These two considerations determine the type of sharp-interface Stefan and kinetic conditions. A one-phase model results for $\delta \ll \epsilon$, and a two-phase model when $\delta = O(\epsilon)$. The sharp-interface kinetic conditions are determined by the reaction-diffusion equations within the thin reaction zone, thus capturing features of the model on smaller length scales (microscales). The resulting sharp-interface model considered as a macroscale model thus contains microscale information, which we argue is more appropriate than simply stating an empirical kinetic condition.

The issue of which diffusivity situation is appropriate, i.e., one or both rapidly varying, is a modeling aspect. The choice will ultimately depend on the best fit with experimental observations for the carbonation zone.

It is worth noting the following open issues:

- In [16, section 1.5 and chapter 9], a class of distributed-microstructure models is derived. This concerns two-scale systems of PDEs which are coupled via micro-macro boundary conditions. [18] and [19] report on such two-scale problems where, at the micro level, a sharp-interface model is responsible for the evolution of micro-free reaction boundaries. Can the two-scale model presented here be derived via such homogenization techniques?
- Are there any connections between the two-scale result of this paper and the localized model-upscaling (LMU) method by Degond, Liu, and Mieussens [8]? LMU is typically used in the context of Boltzmann-like equations. It

consists of coupling a perturbation model and its asymptotic limit model via a transition zone. In the transition zone, the solution is decomposed into a microscopic fraction (described by the perturbation problem) and a macroscopic one (described by the limit problem).

- The single-scale Stefan-like problems can be investigated by means of standard methods for free-boundary problems; see, e.g., [12]. However, the well-posedness of the two-scale FBPs summarized in section 7 is an open problem. We expect that methods developed in [2, 25, 23] and [3] can be adapted to cope with the two-scale structure of the problem presented here.
- Once the limit problems are shown to be well-posed, the next step is to prove rigorously the passing to the limit $\epsilon \to 0$ by obtaining an upper bound on the convergence rate (corrector estimate). This issue is open even for the derivation (as fast-reaction limit) of the standard Stefan problem.
- For the practical corrosion problem, the geometry of the concrete structure plays an important role. We would like to extend the asymptotics to two- and three-dimensional cases and explore the effect of corners on the speed of the moving reaction interface. Resolving numerically in an accurate manner two- and three-dimensional singular-perturbation scenarios requires a good understanding of the evolution of the singular part—the reaction layer. We anticipate that the asymptotic method will aid in constructing a robust method to capture the a priori unknown position of the layer.
- Finally, the two-scale models require validation using, for example, the experimental data reported in [26] or [29]. It is unclear for the moment what the best option is: Should the two-scale sharp-interface model be used or its ϵ-approximation (which is correct only to within a corrector range to be established)?

Appendix A. Stage I carbonation.

A.1. Slowly varying diffusivities. Here we complete the analysis in the case $\delta = O(\epsilon)$ considered in section 4.1.3 for slowly varying diffusivities. The reaction zone remains at the surface until the hydroxide within it is consumed. As such $h = O(1)$, and for this inner region we consider the scalings

$$x = \epsilon^{\frac{2}{p+1}}\bar{x}, \qquad c = \epsilon^{\frac{2}{p+1}}\bar{c}, \qquad h = \bar{h}, \tag{151}$$

giving

$$\epsilon^{\frac{4}{p+1}}\mu\frac{\partial \bar{c}}{\partial t} - \frac{\partial}{\partial \bar{x}}\left(D_c\frac{\partial \bar{c}}{\partial \bar{x}}\right) = -\bar{c}^p\bar{h}^q, \tag{152}$$

$$\epsilon^{\frac{4}{p+1}}\frac{\partial \bar{h}}{\partial t} - \lambda^2\frac{\partial}{\partial \bar{x}}\left(D_h\frac{\partial \bar{h}}{\partial \bar{x}}\right) = -\epsilon^{\frac{2}{p+1}}\bar{c}^p\bar{h}^q. \tag{153}$$

Posing

$$\bar{c} = \bar{c}_0 + \epsilon^{\frac{2}{p+1}}\bar{c}_1 + \cdots, \qquad \bar{h} = \bar{h}_0 + \epsilon^{\frac{2}{p+1}}\bar{h}_1 + \cdots, \tag{154}$$

after an initial transient $t = O(\epsilon^{\frac{4}{p+1}})$, we obtain at the leading order

$$\frac{\partial}{\partial \bar{x}}\left(D_c\frac{\partial \bar{c}_0}{\partial \bar{x}}\right) = \bar{c}_0^p\bar{h}_0^q, \qquad \lambda^2\frac{\partial}{\partial \bar{x}}\left(D_h\frac{\partial \bar{h}_0}{\partial \bar{x}}\right) = 0, \tag{155}$$

subject to

$$\text{at } \bar{x}=0, \qquad D_c\frac{\partial \bar{c}_0}{\partial \bar{x}}=-H, \quad D_h\frac{\partial \bar{h}_0}{\partial \bar{x}}=0, \tag{156}$$

$$\text{as } \bar{x}\to+\infty, \qquad \bar{c}_0\to 0, \quad \bar{h}_0\to h_0(0,t). \tag{157}$$

Consequently,

(158)

$$\bar{h}_0=h_0(0,t), \qquad \bar{c}_0=\begin{cases} \frac{H}{D_c\sigma_p(t)}\left(1+\frac{(p-1)}{2}\sigma_p(t)x\right)^{-\frac{2}{(p-1)}}, & p>1,\\ \frac{H}{D_c\sigma_1(t)}\exp\left(-\sigma_1(t)x\right), & p=1,\\ \left(\left(\frac{H}{D_c\sigma_1(t)}\right)^{\frac{(1-p)}{(1+p)}}-\frac{(1-p)}{2}\sigma_1(t)x\right)^{\frac{2}{(1-p)}}, & 0\le p<1, \end{cases}$$

where

$$\sigma_p(t)=\left(\frac{2h_0(0,t)^q}{(1+p)D_c}\left(\frac{H}{D_c}\right)^{p-1}\right)^{\frac{1}{1+p}}$$

and setting $p=1$ gives $\sigma_1(t)$. This solution recorded for $\bar{c}_0$ is relevant when D_c is constant in this region.

At the next order for the hydroxide, we have

$$\lambda^2\frac{\partial}{\partial \bar{x}}\left(D_h\frac{\partial \bar{h}_1}{\partial \bar{x}}\right)=\bar{c}_0^p\bar{h}_0^q, \tag{159}$$

with

$$\text{at } \bar{x}=0, \qquad D_h\frac{\partial \bar{h}_1}{\partial \bar{x}}=0, \tag{160}$$

giving

$$\lambda^2 D_h\frac{\partial \bar{h}_1}{\partial \bar{x}}=D_c\frac{\partial \bar{c}_0}{\partial \bar{x}}+H. \tag{161}$$

The leading order outer 2 problem is thus the fixed domain problem

$$\text{in } 0<x<1,\ t>0, \qquad \frac{\partial h_0}{\partial t}=\lambda^2\frac{\partial}{\partial x}\left(D_h\frac{\partial h_0}{\partial x}\right), \tag{162}$$

$$\text{at } x=0, \qquad \lambda^2 D_h\frac{\partial h_0}{\partial x}=H, \tag{163}$$

$$\text{at } x=1, \qquad D_h\frac{\partial h_0}{\partial x}=0, \tag{164}$$

$$\text{at } t=0, \qquad h_0=h_i \quad \text{for } 0\le x\le 1, \tag{165}$$

the condition (163) following from matching with the above two-term inner solution (154) and using (161). In the case when D_h and h_i are constants, we have the explicit solution

$$h_0(x,t)=h_i-Ht+\frac{H}{\lambda^2 D_h}\left(\frac{x}{2}(2-x)+\sum_{n=0}^{\infty}f_n\exp(-\lambda^2 D_h n^2\pi^2 t)\cos(n\pi x)\right), \tag{166}$$

where the Fourier coefficients are

$$f_0 = \frac{1}{3}, \qquad f_n = \frac{2}{n^2\pi^2} \text{ for } n \geq 1. \tag{167}$$

In the semi-infinite case, the corresponding solution is

$$h_0(x,t) = h_i - \frac{H}{\lambda D_h^{\frac{1}{2}}} \int_0^t \frac{\exp(-x^2/4\lambda^2 D_h s)}{\sqrt{\pi s}} ds. \tag{168}$$

We denote by $t = t_0$ the time at which the leading order hydroxide concentration falls to zero at the reaction zone, i.e., $h_0(0,t) = 0$, the resulting concentration profile then being $H_i(x) = h_0(x,t_0)$. In the finite domain case, (166) gives a transcendental equation for t_0,

$$Ht_0 = h_i + \frac{H}{\lambda^2 D_h} \sum_{n=0}^{\infty} f_n \exp(-\lambda^2 D_h n^2 \pi^2 t_0), \tag{169}$$

with then

$$H_i(x) = h_i - Ht_0 + \frac{H}{\lambda^2 D_h} \left(\frac{1}{2} x(2-x) + \sum_{n=0}^{\infty} f_n \exp(-\lambda^2 D_h n^2 \pi^2 t_0) \cos(n\pi x) \right). \tag{170}$$

In the semi-infinite domain case, (168) gives explicitly

$$t_0 = \frac{\pi \lambda^2 D_h h_i^2}{4H^2}, \qquad H_i(x) = h_i - \frac{H}{\lambda D_h^{\frac{1}{2}}} \int_0^{t_0} \frac{\exp(-x^2/4\lambda^2 D_h s)}{\sqrt{\pi s}} ds. \tag{171}$$

Since the leading order inner solution for the hydroxide $\bar{h}_0$ does not vary spatially within the inner region, this stage I carbonation persists until the leading order outer 2 solution falls to zero at the reaction zone. Subsequently stage II carbonation takes place as described in section 4.1.3.

The case $H = \infty$ is different from the above, since c as well as h are now order 1 in the reaction zone.

A.2. Single rapidly varying diffusivity D_c. For the single rapidly varying CO_2 diffusivity considered in section 5.1.3, a stage I carbonation regime takes place analogous to the slowly varying case. The CO_2 diffusivity is now small in the reaction zone; consequently the scalings (151) change to

$$x = \epsilon^{\frac{4}{p+1}} \bar{x}, \qquad c = \epsilon^{\frac{4}{p+1}} \bar{c}, \qquad h = \bar{h}, \qquad D_c = \epsilon^2 \bar{D}_c, \tag{172}$$

and the expansion is modified to

$$\bar{c} = \bar{c}_0 + \epsilon^{\frac{4}{p+1}} \bar{c}_1 + \cdots, \qquad \bar{h} = \bar{h}_0 + \epsilon^{\frac{4}{p+1}} \bar{h}_1 + \cdots. \tag{173}$$

The rest of the analysis remains similar, with D_c replaced by $\bar{D}_c$, which we note for the specific form (63) is $\bar{D}_c = \nu_1 / h_0(0^+,t)^q$. This pertains until $h_0(0^+,t)$ falls $O(\epsilon^{2/q})$, the waiting time t_0 being the same in this case.

Appendix B. The inner 1 asymptotics. We complete here the analysis of the inner 1 region in section 5.1.1 for the parameter regime $0 < q \leq 1$.

In the case $q = 1$, this inner 1 region is the same size as the inner inner region, although located in its far-field. We scale using

$$x = s(t) + \epsilon^2(S(t) + \hat{x}), \qquad c = \hat{c}, \qquad h = \epsilon^2\hat{h}, \tag{174}$$

where $1 \ll S(t) \ll 1/\epsilon^2$. The governing equations become

$$\epsilon^4\mu\frac{\partial\hat{c}}{\partial t} - \epsilon^2\mu(\dot{s} + \epsilon^2\dot{S})\frac{\partial\hat{c}}{\partial\hat{x}} - \frac{\partial}{\partial\hat{x}}\left(D_c\frac{\partial\hat{c}}{\partial\hat{x}}\right) = -\epsilon^4\hat{c}^p\hat{h}^q, \tag{175}$$

$$\epsilon^2\frac{\partial\hat{h}}{\partial t} - (\dot{s} + \epsilon^2\dot{S})\frac{\partial\hat{h}}{\partial\hat{x}} - \lambda^2\frac{\partial}{\partial\hat{x}}\left(D_h\frac{\partial\hat{h}}{\partial\hat{x}}\right) = -\hat{c}^p\hat{h}^q. \tag{176}$$

Posing (73) with $q = 1$, we obtain (74), with the equation for $\hat{h}_0$ being

$$\dot{s}\frac{\partial\hat{h}_0}{\partial\hat{x}} + \lambda^2\frac{\partial}{\partial\hat{x}}\left(D_h\frac{\partial\hat{h}_0}{\partial\hat{x}}\right) = \hat{c}_0^p\hat{h}_0^q. \tag{177}$$

After matching to outer 1 and the inner inner, we again obtain (75) with $\hat{h}_0$ and $S(t)$ (in the case D_h constant) given by

$$\hat{h}_0 = \exp\left(\sigma(t)\hat{x}\right), \qquad S(t) \sim \frac{2}{q\sigma(t)}\log(\epsilon), \tag{178}$$

where

$$\sigma(t) = \frac{-\dot{s} + (\dot{s}^2 + 4\lambda^2 D_h c_0(s^-, t)^p)^{\frac{1}{2}}}{2\lambda^2 D_h}.$$

In the case $0 < q < 1$, the inner 1 region is smaller than the inner inner. We scale using

$$x = s(t) + \epsilon^2\left(S(t) + \epsilon^{\frac{1-q}{q}}\hat{x}\right), \qquad c = \hat{c}, \qquad h = \epsilon^{\frac{2}{q}}\hat{h}, \tag{179}$$

where $S(t) \le 0$ can be taken as the location at which the inner inner solution $\bar{h}_0$ first becomes zero. We thus obtain

$$\epsilon^{\frac{2(1+q)}{q}}\mu\frac{\partial\hat{c}}{\partial t} - \epsilon^{\frac{(1+q)}{q}}\mu(\dot{s} + \epsilon^2 S(t))\frac{\partial\hat{c}}{\partial\hat{x}} - \frac{\partial}{\partial\hat{x}}\left(D_c\frac{\partial\hat{c}}{\partial\hat{x}}\right) = -\epsilon^{\frac{2(1+q)}{q}}\hat{c}^p\hat{h}^q, \tag{180}$$

$$\epsilon^{\frac{2}{q}}\frac{\partial\hat{h}}{\partial t} - \epsilon^{\frac{1-q}{q}}(\dot{s} + \epsilon^2 S(t))\frac{\partial\hat{h}}{\partial\hat{x}} - \lambda^2\frac{\partial}{\partial\hat{x}}\left(D_h\frac{\partial\hat{h}}{\partial\hat{x}}\right) = -\hat{c}^p\hat{h}^q. \tag{181}$$

Posing

$$\hat{c} \sim \hat{c}_0 + \epsilon^{\frac{(1+q)}{q}}\hat{c}_1, \qquad \hat{h} \sim \hat{h}_0, \tag{182}$$

we again obtain (74), with the equation for $\hat{h}_0$ now being

$$\lambda^2\frac{\partial}{\partial\hat{x}}\left(D_h\frac{\partial\hat{h}_0}{\partial\hat{x}}\right) = \hat{c}_0^p\hat{h}_0^q. \tag{183}$$

Matching to outer 1 and the inner inner gives (75), with $\hat{h}_0$ (in the case D_h constant) given by

$$\hat{h}_0 = \begin{cases} \left(\frac{(1-q)^2 c_0(s^-,t)^p}{2(1+q)\lambda^2 D_h}\hat{x}^2\right)^{\frac{1}{1-q}} & \text{for } \hat{x} > 0, \\ 0 & \text{for } \hat{x} < 0. \end{cases} \tag{184}$$

REFERENCES

[1] D. Agreba-Driolett, F. Diele, and R. Natalini, *A mathematical model for the sulphur dioxide aggression to calcium carbonate stones: Numerical approximation and asymptotic analysis*, SIAM J. Appl. Math., 64 (2004), pp. 1636–1667.

[2] T. Aiki and A. Muntean, *Existence and uniqueness of solutions to a mathematical model predicting service life of concrete structures*, Adv. Math. Sci. Appl., 19 (2009), pp. 109–129.

[3] T. Aiki and A. Muntean, *Large time behavior of solutions to a moving-interface problem modeling concrete carbonation*, Comm. Pure Appl. Anal., 9 (2010), pp. 1117–1129.

[4] K. Y. Ann, S.-W. Pack, J.-P. Hwang, H.-W. Song, and S.-H. Kim, *Service life prediction of a concrete bridge structure subjected to carbonation*, Construct. Building Materials, 24 (2010), pp. 1494–1501.

[5] C. M. Bender and S. A. Orszag, *Advanced Mathematical Methods for Scientists and Engineers*, Springer-Verlag, Berlin, 1999.

[6] T. Chaussadent and V. Baroghel-Bouny, *Transfers between Concrete and Structural Durability. Overview of Five Years of Research and Outlook for the Future*, technical report, Lab. Central de Ponts et Chausees, 2004.

[7] P. V. Danckwerts, *Gas-Liquid Reactions*, McGraw–Hill, New York, 1970.

[8] P. Degond, J.-G. Liu, and L. Mieussens, *Macroscopic fluid models with localized kinetic upscaling effects*, Multiscale Model. Simul., 5 (2006), pp. 940–979.

[9] J. D. Evans and J. R. King, *Asymptotic results of the Stefan problem with kinetic undercooling*, Quart. J. Mech. Appl. Math., 53 (2000), pp. 449–473.

[10] J. D. Evans and J. R. King, *On the derivation of heterogeneous reaction kinetics from a homogeneous reaction model*, SIAM J. Appl. Math., 60 (2000), pp. 1977–1996.

[11] J. D. Evans and J. R. King, *The Stefan problem with nonlinear kinetic undercooling*, Quart. J. Mech. Appl. Math., 56 (2003), pp. 139–161.

[12] A. Fasano and M. Primicerio, *General free-boundary problems for the heat equation.* I., J. Math. Anal. Appl., 57 (1977), pp. 694–723.

[13] T. Fatima, N. Arab, E. P. Zemskov, and A. Muntean, *Homogenization of a reaction-diffusion system modeling sulfate corrosion in locally periodic perforated domains*, J. Engrg. Math., 69 (2010), pp. 261–276.

[14] V. A. Galaktionov, J. Hulshof, and J. L. Vazquez, *Extinction and focusing behaviour of spherical and annular flames described by a free boundary problem*, J. Math. Pures Appl. (9), 76 (1997), pp. 563–608.

[15] P. S. Hagan, R. S. Polizzotti, and G. Luckman, *The effects of surface poisons on the oxidation of binary alloys*, SIAM J. Appl. Math., 45 (1985), pp. 826–842.

[16] U. Hornung, *Homogenization and Porous Media*, Springer-Verlag, New York, 1997.

[17] J. Kropp, *Relations between transport characteristics and durability*, RILEM, 1995, in Performance Criteria for Concrete Durability.

[18] S. A. Meier, *Two-Scale Models for Reactive Transport and Evolving Microstructures*, Ph.D. thesis, University of Bremen, Bremen, Germany, 2008.

[19] S. A. Meier and A. Muntean, *A two-scale reaction-diffusion system with micro-cell reaction concentrated on a free boundary*, C. R. Mécanique, 336 (2009), pp. 481–486.

[20] S. A. Meier, M. A. Peter, A. Muntean, and M. Böhm, *Dynamics of the internal reaction layer arising during carbonation of concrete*, Chem. Eng. Sci., 62 (2007), pp. 1125–1137.

[21] A. Muntean, *A Moving-Boundary Problem: Modeling, Analysis and Simulation of Concrete Carbonation*, Ph.D. thesis, University of Bremen, Bremen, Germany, 2006.

[22] A. Muntean, *On the interplay between fast reaction and slow diffusion in the concrete carbonation process: A matched-asymptotics approach*, Meccanica, 44 (2009), pp. 35–46.

[23] A. Muntean, *Well-posedness of a moving-boundary problem with two moving reaction strips*, Nonlinear Anal. Real World Appl., 10 (2009), pp. 2541–2557.

[24] A. Muntean and M. Böhm, *Interface conditions for fast-reaction fronts in wet porous mineral materials: The case of concrete carbonation*, J. Engrg. Math., 65 (2009), pp. 89–100.

[25] A. Muntean and M. Böhm, *A moving-boundary problem for concrete carbonation: Global existence and uniqueness of weak solutions*, J. Math. Anal. Appl., 350 (2009), pp. 234–251.
[26] A. Muntean, M. Böhm, and J. Kropp, *Moving carbonation fronts in concrete: A moving-sharp-interface approach*, Chem. Eng. Sci., 66 (2011), pp. 538–546.
[27] C. V. Nikolopoulos, *A mushy region in concrete corrosion*, Appl. Math. Model., 34 (2010), pp. 4012–4030.
[28] P. Ortoleva, E. Merino, C. Moore, and J. Chadam, *Geochemical self-organization* I; *Reaction-transport feedbacks and modeling approach*, Amer. J. Sci., 287 (1987), pp. 979–1007.
[29] V. G. Papadakis, C. G. Vayenas, and M. N. Fardis, *A reaction engineering approach to the problem of concrete carbonation*, AIChE, 35 (1989), pp. 1639–1650.
[30] V. G. Papadakis, C. G. Vayenas, and M. N. Fardis, *Fundamental modeling and experimental investigation of concrete carbonation*, ACI Materials J., 88 (1991), pp. 363–373.
[31] A. V. Saetta and R. V. Vitaliani, *Experimental investigation and numerical modeling of carbonation process in reinforced concrete structures: Part* I: *Theoretical formulation*, Cement and Concrete Res., 34 (2004), pp. 571–579.
[32] H. F. W. Taylor, *Cement Chemistry*, Academic Press, London, 1990.